FBXO7/ntc and USP30 antagonistically set the ubiquitination threshold for basal mitophagy and provides a target for Pink1 phosphorylation *in vivo*

Alvaro Sanchez-Martinez[1]*, Aitor Martinez[1], Alexander J. Whitworth[1]*

[1]MRC Mitochondrial Biology Unit, University of Cambridge, Cambridge Biomedical Campus, Hills Road, Cambridge, CB2 0XY, United Kingdom.

*Correspondence should be addressed to A.S.M. (e-mail alvaro.sanchez@mrc-mbu.cam.ac.uk) or A.J.W. (e-mail a.whitworth@mrc-mbu.cam.ac.uk)

Short title: FBXO7/ntc regulates basal mitophagy *in vivo*

Key words: FBXO7, ntc, PINK1, Parkin, USP30, pS65-Ub, mitophagy, Parkinson's Disease

Abstract

Functional analyses of genes linked to heritable forms of Parkinson's disease (PD) have revealed fundamental insights into the biological processes underpinning pathogenic mechanisms. Mutations in *PARK15/FBXO7* cause autosomal recessive PD and FBXO7 has been shown to regulate mitochondrial homeostasis. We investigated the extent to which FBXO7 and its *Drosophila* orthologue, ntc, share functional homology and explored its role in mitophagy *in vivo*. We show that *ntc* mutants partially phenocopy *Pink1* and *parkin* mutants and *ntc* overexpression supresses *parkin* phenotypes. Furthermore, ntc can modulate basal mitophagy in a Pink1- and parkin-independent manner by promoting the ubiquitination of mitochondrial proteins, a mechanism that is opposed by the deubiquitinase USP30. This basal ubiquitination serves as the substrate for Pink1-mediated phosphorylation which triggers stress-induced mitophagy. We propose that FBXO7/ntc works in equilibrium with USP30 to provide a checkpoint for mitochondrial quality control in basal conditions *in vivo* and presents a new avenue for therapeutic approaches.

Introduction

Parkinson's disease (PD) is the second most common neurodegenerative disorder. Autosomal recessive mutations in the genes encoding the mitochondrial kinase PINK1 (*PINK1*) and the E3 ubiquitin ligase Parkin (*PRKN*) are associated with early-onset parkinsonism. These genes have been shown to function in a common mitochondrial quality control pathway whereby mitochondria are degraded by autophagy (mitophagy). Briefly, PINK1 is partially imported to healthy polarised mitochondria where it is cleaved and subsequently degraded in the cytosol (1). Upon mitochondrial depolarisation, PINK1 is stabilised on the outer mitochondrial membrane (OMM) where it phosphorylates ubiquitin-Ser65 (pS65-Ub) conjugated to OMM proteins (2, 3). This acts as a signal for Parkin to be recruited and phosphorylated, relieving its autoinhibitory conformation, and allowing it to further ubiquitinate OMM proteins in close proximity (4, 5) that will serve as additional substrates for PINK1 creating a feed-forward mechanism (6). Counteracting mitochondrial ubiquitination, USP30, a mitochondrial outer membrane deubiquitinase, removes ubiquitin (Ub) from Parkin substrates acting as a negative regulator of mitophagy (7). The accumulation of pS65-Ub on the OMM triggers the recruitment of autophagy receptors, which promote autophagosome recruitment and, ultimately, degradation of the damaged mitochondria (8, 9).

However, most of our understanding of the function of PINK1 and Parkin come from the utilisation of mitochondrial uncouplers or inhibitors in cultured cells, usually in conjunction with Parkin overexpression (8, 10). Hence, there is a need to understand these mechanisms in more physiological model systems. *Drosophila melanogaster* models have delivered fundamental insights into the physiological function of the homologues *Pink1* and *parkin* (adopting FlyBase nomenclature), providing an excellent system to study mitochondrial homeostasis (11-16). Interestingly, while proteomic analysis of mitochondrial turnover in *Drosophila* supports a role of Pink1/parkin in mitochondrial quality control (17), studies using pH-sensitive fluorescent mitophagy reporters showed that Pink1 and parkin had minimal impact on basal mitophagy (18-21). Thus, many questions endure regarding the mechanisms of action of Pink1/parkin in mitochondrial quality control *in vivo* and the potential contribution of other key players.

Mutations in the gene encoding F-box protein 7 (*FBXO7)*, have been found to cause autosomal recessive early-onset parkinsonism similar to those caused by mutations in *PINK1* and *PRKN* (22, 23), motivating a need to understand how FBXO7 is related to PINK1/Parkin biology. F-box domain-containing proteins are essential factors of the SCF-type (Skp1-Cul1-F-box) E3-ubiquitin ligase complexes, which are responsible for recruiting Ub target substrates via the F-box domain (24). FBXO7 has both SCF-dependent and SCF-independent activities (25, 26). Although it has been previously shown to cooperate with PINK1 and Parkin in mitophagy (27), how this occurs *in vivo* is poorly characterised warranting further investigation in an animal model. *Drosophila* encode a single homologue of *FBXO7* called *nutcracker* (*ntc*), which was identified in a screen for genes that control caspase activation during a late stage of spermatogenesis (28). ntc shares sequence, structure, and some functional similarities with mammalian FBXO7 (26, 28, 29) and has been shown to regulate proteasome function via its binding partner PI31, an interaction that is conserved in FBXO7 (28, 29). Thus, *Drosophila* provides a genetically tractable system to study role of ntc/FBXO7 in mitochondrial quality control *in vivo*.

Mitochondrial quality control mechanisms are believed to have an important pathophysiological role in PD. However, how this process is orchestrated *in vivo* and the upstream factors involved are still unclear. Therefore, we sought to investigate the relationship between ntc, Pink1 and parkin, and their role in mitophagy, in particular basal mitophagy. We have found that ntc is able to compensate for the absence of *parkin* but not *Pink1*. Moreover, ntc plays an important role in promoting basal

91 mitophagy in a Pink1- and parkin-independent manner, which is opposed by its
92 counteracting partner USP30. This mechanism sets a threshold for basal mitophagy
93 by regulating the steady-state levels of ubiquitin on OMM proteins, subsequently
94 modulating the levels of pS65-Ub. Together, we provide evidence of a novel
95 checkpoint for basal mitophagy that could potentially serve as therapeutic target for
96 neurodegenerative disorders.
97
98
99 **Results**
100
101 **Overexpression of *ntc* can rescue parkin but not Pink1 mutant phenotypes**
102 The F-box domain localised in the C-terminal of *Drosophila* ntc shares considerable
103 sequence similarity with that of human FBXO7 (28). Both proteins have a conserved
104 valine residue involved in substrate recognition, including common interacting
105 partners, e.g. PI31 (26, 29). However, a functional conservation in between FBXO7
106 and ntc has not been formally tested *in vivo.* Notably, it has been shown that FBXO7
107 functionally interacts with mammalian PINK1 and Parkin and genetically interacts with
108 *parkin* in *Drosophila* (27). Therefore, as an initial exploration of the functional homology
109 between ntc and FBXO7, we tested for a similar genetic interaction between *ntc* and
110 *parkin. Drosophila parkin* mutants present multiple disease-relevant phenotypes,
111 including locomotor deficits, dopaminergic neurodegeneration, and a severe
112 mitochondrial disruption leading to flight muscle degeneration (13, 14). Strikingly,
113 overexpression of *ntc* by the strong ubiquitous *daughterless* (*da*)-GAL4 driver
114 significantly rescued these *parkin* phenotypes, (Figure 1A-1D). At the molecular level,
115 we observed that ntc is also able to decrease the steady state levels of the *Drosophila*
116 Mitofusin (MFN1/MFN2) homologue, Marf, which has been previously shown to be
117 increased in *parkin* mutants (16) (Figure 1E). These results support a functional
118 homology between FBXO7 and ntc, and, moreover, indicate that ntc can at least
119 partially substitute for parkin *in vivo*.
120
121 In contrast, assessing the functional relationship between ntc and Pink1 in a similar
122 manner, *ntc* overexpression was unable to rescue climbing or flight locomotor defects
123 of *Pink1* mutants, nor the increased Marf steady-state levels (Figure 1F-1H).
124 Furthermore, the neurodegenerative 'rough eye' phenotype – commonly used for
125 testing genetic interactors (30, 31) – induced by *Pink1* overexpression, in a robustly
126 stereotyped manner, was not enhanced by *ntc* overexpression as previously shown

127 for *parkin* (15). These results mirror equivalent analyses of *FBXO7* (27), and indicate
128 that *Pink1* and *ntc* do not obviously genetically interact.
129

130 ***ntc* mutants partially phenocopy *Pink1/parkin* mutants**

131 If ntc performs similar functions to the Pink1/parkin pathway in *Drosophila*, we
132 reasoned that *ntc* mutants may phenocopy *Pink1/parkin* mutants. Supporting this, *ntc*
133 mutants, like *Pink1* and *parkin* mutants, are male sterile due to defective sperm
134 individualization (11-13, 28, 32). To extend this, we assessed *ntc* mutants for classic
135 *Pink1/parkin* phenotypes as described above. *ntc* mutants homozygous for an
136 amorphic nonsense mutation (ntc^{ms771}; abbreviated as $ntc^{-/-}$) showed a marked defect
137 in climbing and flight ability (Figure 2A, 2B). We verified this was likely specific to *ntc*
138 by assessing a hemizygous condition ($ntc^{-/Df}$) with comparable results (Figure 2A, 2B).
139 Importantly, transgenic re-expression of *ntc* was able to significantly rescue the
140 climbing and flight deficit (Figure 2A, 2B), confirming that the phenotype is specifically
141 caused by loss of ntc function. Also similar to *Pink1/parkin* mutants, *ntc* mutants
142 showed a dramatically shortened lifespan, with median survival of ~7 days compared
143 to ~55 days for controls (Figure 2C), which was almost completely rescued by
144 transgenic re-expression of *ntc* (Figure 2C).
145

146 However, in contrast to *Pink1/parkin* mutants, we did not observed loss of DA neurons
147 in the PPL1 clusters of *ntc* mutants, although the short lifespan limited the analysis to
148 only 10-day-old flies (Figure 2D). Likewise, immunohistochemical analyses of *ntc*
149 mutants revealed no apparent disruption of mitochondrial morphology or integrity at
150 confocal or electron-microscopy levels in flight muscle (Figure 2E) or larval central
151 nervous system (CNS) (Figure 2F). Analysing mitochondrial respiratory capacity, *ntc*
152 mutants were not consistently different from controls despite a downward trend (Figure
153 2G). Nevertheless, ATP levels were reduced in *ntc* mutants (Figure 2H), which was
154 rescued by re-expression of wild-type *ntc*.
155

156 Oxidative stress is a consistent feature of PD pathology and normal ageing. Many
157 models of PD show sensitivity to oxidative stressors such as paraquat (PQ), including
158 *Drosophila parkin* mutants (33, 34). Similarly, *ntc* mutants also showed increased
159 sensitivity to PQ exposure (Figure 2I). Together, these results show that loss of *ntc*
160 causes previously undescribed phenotypes that impact organismal vitality similar to,
161 but also different from, *Pink1/parkin* mutants, though the effects are generally less
162 severe.

163

164 **ntc regulates basal mitophagy and antagonises USP30 in a Pink1/parkin-**
165 **independent manner**

166 Previous work showed that FBXO7 facilitates PINK1/Parkin-mediated mitophagy upon
167 mitochondrial depolarisation in cultured cells (27). Thus, we next sought to determine
168 whether *Drosophila* ntc acts to promote mitophagy *in vivo*. The *mito*-QC reporter
169 provides a sensitive and robust reporter for mitophagy whereby the GFP of OMM-
170 localised tandem mCherry-GFP is quenched in the acidic lysosome, revealing
171 mitolysosomes as 'mCherry-only' puncta (35). Importantly, in the absence of potent
172 mitochondrial toxins – not readily applicable *in vivo* – the steady-state analysis of *mito*-
173 QC provides an insight into basal mitophagy (20, 36). Quantifying basal mitophagy in
174 larval neurons revealed a significant reduction in *ntc* mutants compared to controls,
175 which was rescued upon re-expression of *ntc* (Figure 3A, 3B). Conversely, *ntc*
176 overexpression significantly increased basal mitophagy (Figure 3C, 3D). To verify
177 these results, we analysed an alternative mitophagy reporter with a mitochondrial
178 matrix-targeted version of *mito-QC*, termed *mtx-QC*, with equivalent results (Figure
179 S1A, S1B). Thus, ntc is both necessary and sufficient to promote basal mitophagy.
180 Similarly, transgenic expression of *FBXO7* also increased mitophagy in larval neurons,
181 underscoring their shared functionality (Figure S2A, S2B). Further validating these
182 results in human cells stably expressing the *mito*-QC reporter (37), siRNA-mediated
183 knockdown of *FBXO7* also significantly reduced basal mitophagy (Figure S2C-S2E).
184 Together these results support a conserved function of FBXO7/ntc in regulating basal
185 mitophagy.

186

187 While stress-induced mitophagy has been extensively studied, especially in cultured
188 cell lines, mechanisms regulating basal mitophagy are poorly characterised *in vivo*.
189 Under basal conditions loss of *USP30*, an established regulator of mitophagy, leads to
190 accumulation of ubiquitinated OMM proteins, and sustained *USP30* loss or inhibition
191 promotes mitophagy *in vitro* (38-42), but *in vivo* characterisation remains limited. Upon
192 *USP30* knockdown we observed a significant increase in basal mitophagy in larval
193 neurons, using both the *mito-QC* (Figure 3E, 3F) and *mtx-QC* reporters (Figure S1A,
194 S1B), and in adult flight muscle (Figure S3A, S3B). These results indicate that USP30
195 indeed inhibits basal mitophagy *in vivo* as expected. Importantly, we found that the
196 induction of basal mitophagy by loss of *USP30* requires the activity of ntc as it was
197 abolished in a *ntc* mutant background (Figure 3E, 3F).

198

199 As an orthogonal approach to test for genetic interaction at the organismal level, we
200 found that while *USP30* knockdown did not cause any gross defect in adult viability or
201 behaviour (Figure S3C), *USP30* overexpression caused a locomotor defect (Figure
202 3G). This phenotype was completely suppressed by co-expression of *ntc* (Figure 3G),
203 consistent with the opposing actions of Ub-ligase and deubiquitinase and supporting
204 the idea of ntc acting upstream of USP30. Interestingly, while *parkin* overexpression
205 also suppressed the *USP30* overexpression phenotype as expected (Figure S3D),
206 other Ub-ligases linked to mitophagy, Mul1 and March5 (39, 43-47), showed no
207 suppression of this phenotype (Figure S3D). Moreover, similar to *parkin* loss (20) or
208 overexpression (Figure S3E, S3F), loss of Mul1 or March5 had no effect on basal
209 mitophagy (Figure S3G-S3J). Together, these data highlight the specificity of ntc and
210 USP30 as important and opposing regulators of basal mitophagy.
211
212 Given the previously established links between FBXO7 and USP30 with toxin-induced
213 PINK1/Parkin mitophagy in cultured human cells, we next analysed whether the
214 induction of basal mitophagy by *ntc* overexpression or *USP30* knockdown involved the
215 *Pink1/parkin* pathway *in vivo*. As previously reported (20), the absence of *parkin* or
216 *Pink1* did not impact basal mitophagy in larval neurons (Fig 4A-D). However,
217 overexpression of *ntc* was still able to induce mitophagy in the absence of either *parkin*
218 or *Pink1* (Figure 4A-4D). Likewise, *USP30* knockdown also increased mitophagy
219 independently of *parkin* and *Pink1* (Figure 5A-5D), consistent with *in vitro* findings (38,
220 39, 48, 49). Notably, the induction of mitophagy by *USP30* knockdown in *Pink1* or
221 *parkin* mutant backgrounds required the function of *ntc* (Fig 5A-D), further
222 underscoring the importance of ntc in basal mitophagy.
223
224 **General autophagy is not grossly affected upon USP30 or ntc manipulations**
225 Although previously validated as a reliable mitophagy reporter *in vivo*, we nevertheless
226 verified that the increased mitolysosome formation (mitophagy) by *ntc* overexpression
227 or *USP30* knockdown occurs via canonical autophagy flux as it was abrogated in the
228 absence of *Atg8a*, the main fly homologue of human ATG8 family members
229 GABARAP/LC3, in both wild-type or *parkin* mutant backgrounds (Figure S4A-S4D).
230 Notwithstanding, the observed increase in mitolysosomes could be due to an increase
231 in non-selective autophagy (50, 51). Thus, we used a number of well-established
232 orthogonal assays to assess the effect of these mitophagy-inducing manipulations on
233 general autophagy.
234

First, we examined the level of lipidated Atg8a (Atg8a-II) which is incorporated into autophagosomal membranes and is used as an indication of autophagy induction (52, 53). Neither *USP30* knockdown, *ntc* overexpression nor *ntc* loss had any effect on autophagy induction (Figure 6A, 6B). Similarly, the steady-state levels of ref(2)P, the homologue of mammalian p62, which accumulates upon autophagic blockage (54), was also not affected in any of the conditions (Figure 6C, 6D). We also analysed the autophagy flux reporter GFP-mCherry-Atg8a (55-57). Quantification of mCherry-Atg8a puncta (autolysosomes) showed no changes upon manipulating levels of *USP30* or *ntc* (Figure 6E, 6F). Together, these results support that the effect observed upon manipulation of *USP30* or *ntc* is specific for basal mitophagy and not a consequence of altered general autophagic flux.

ntc increases basal mitochondrial ubiquitin and promotes phospho-ubiquitin formation

To gain a mechanistic insight into the regulation of basal mitophagy by ntc and USP30, we analysed their impact on mitochondrial ubiquitination. Consistent with their molecular functions, both *ntc* overexpression and *USP30* knockdown increased the total amount of ubiquitin present in mitochondria-enriched fractions under basal conditions (Figure 7A-B, Figure S5A), while total Ub remained unchanged (Figure S5B). Indeed, recent studies indicate that USP30 acts to remove pre-existing OMM ubiquitin under basal conditions, influencing the threshold needed for Parkin activation (38, 58).

We have recently described that loss of *parkin* causes a significant accumulation of pS65-Ub, consistent with parkin promoting the degradation of pS65-Ub labelled mitochondria (59). Unlike loss of *parkin*, loss of *ntc* alone did not lead to pS65-Ub build up (Figure 7C, 7D). However, *parkin*:*ntc* double mutants result in a significant reduction in the accumulated pS65-Ub levels (Figure 7C, 7D), and overexpression of *ntc* in the *parkin* mutant background increased the amount of pS65-Ub compared to *parkin* mutants alone (Figure 7E, 7F). These results are consistent with ntc promoting basal mitochondrial ubiquitination, which is phosphorylated by Pink1 to drive mitophagy. Thus, together these data suggest that ntc and USP30 work antagonistically to set up an OMM ubiquitin threshold needed for subsequent mitochondrial clearance.

Discussion

272 Mutations in *FBXO7* have been linked to familial parkinsonism but the mechanisms of
273 pathogenesis are poorly understood (22, 23). We have characterized the putative
274 *Drosophila* homologue, *ntc*, to assess the functional homology with *FBXO7* and its
275 potential as a model to understand the function of FBXO7 *in vivo*.
276
277 FBXO7 has been genetically linked to *Drosophila Pink1* and *parkin* and shown to
278 facilitate PINK1/Parkin-mediated mitophagy *in vitro*. The *Drosophila* models have
279 provided valuable insights into Pink1/parkin biology and genetic interactors have
280 highlighted complementary pathways in mitochondrial homeostasis. Here we show
281 that *ntc* mutants partially phenocopy *Pink1/parkin* phenotypes in locomotor function,
282 lifespan and sensitivity to paraquat, consistent with a role in mitochondria quality
283 control. We also observed the same genetic relationship as previously reported for
284 *FBXO7* (27); namely, that overexpression of *ntc* can rescue all *parkin* mutant
285 phenotypes but not for *Pink1* mutants. It is worth noting that in our previous study (27)
286 we performed an initial characterisation of *ntc* as the putative homologue of *FBXO7*
287 but observed no phenotypes reminiscent of *Pink1/parkin* mutants and provisionally
288 concluded that ntc was not a functional homologue of FBXO7. However, these
289 analyses were conducted using a hypomorphic allele (ntc^{f07259}) in homozygosity,
290 weakening the phenotype penetrance. In the current study, we have conducted our
291 analyses with an amorphic allele, in parallel to studies comparing transgenic
292 expression of *ntc* with *FBXO7*, hence supporting a functional homology between ntc
293 and FBXO7.
294
295 Importantly, FBXO7 has previously been shown to facilitate the PINK1/Parkin pathway
296 to promote stress-induced mitophagy *in vitro* (27, 60). However, whether it regulates
297 mitophagy *in vivo* is poorly characterised. Indeed, mitophagy itself can occur via
298 different regulators and stimuli, and represents only one of several mechanisms of
299 mitochondrial quality control (61, 62). For instance, most studies have utilised a
300 mitochondrial toxification stimulus to model substantial 'damage', however, basal
301 mitophagy occurs as a housekeeping-type mechanism to regulate quantity or
302 piecemeal turnover. The development of genetically encoded mitophagy reporters has
303 provided a powerful approach to monitor both stress-induced or basal mitophagy *in*
304 *vivo*. We have shown here that ntc is able to modulate basal mitophagy in a
305 Pink1/parkin-independent manner, which is conserved by FBXO7 in human cell lines.
306
307 In comparison to stress-induced mitophagy, the regulation of basal mitophagy is poorly
308 characterised, particularly in metazoa. While early studies showed the mitochondrial

309 deubiquitinase USP30 antagonises PINK1/Parkin-mediated mitophagy (41, 63, 64),
310 recent studies have established a role in basal mitophagy (38-40, 42). The emerging
311 view suggests the main role of USP30 is acting as part of a quality control process for
312 intra-mitochondrial proteins during import through the translocon (39, 42), and that
313 basal mitochondrial ubiquitination provides the initiating substrate for PINK1 signalling.
314 This paradigm requires a Ub ligase to provide basal ubiquitination that USP30 acts
315 upon. While Phu et al. (42) suggested that this may be mediated via March5, this was
316 not concurred by Ordureau et al. (39). Thus, the ligase providing the basal
317 ubiquitination is unclear, and the role of USP30 in basal mitophagy *in vivo* remained
318 to be established.
319
320 Here we demonstrated that knockdown of USP30 *in vivo* does indeed increase basal
321 mitophagy in neurons and muscle, consistent with the *in vitro* studies. This also
322 established a paradigm for a more deeply analysis of ntc's function in basal mitophagy.
323 While the induction of basal mitophagy by *USP30* knockdown is Pink1/parkin-
324 independent as expected, it nevertheless required the function of ntc. In contrast,
325 overexpression of parkin or depletion of either Mul1 or March5 did not affect neuronal
326 basal mitophagy in our assay. The antagonistic relationship between USP30 and
327 parkin was also evident from genetic interactions at the organismal level (rescue of a
328 climbing defect), as expected, and was recapitulated with ntc. Such an interaction was
329 also not evident with Mul1 and March5. Mechanistically, we found that *ntc* promotes
330 mitochondrial ubiquitination under basal conditions, which was mirrored by the
331 downregulation of *USP30*, consistent with the idea that basal ubiquitination signals
332 basal mitophagy. Thus, our data suggest that ntc/FBXO7 provides basal ubiquitination,
333 that is antagonised by USP30, which facilitates basal mitophagy upon a yet unclear
334 stimulus.
335
336 The current mechanistic view of PINK1/Parkin stress-induced mitophagy signalling
337 posits that upon mitochondrial depolarisation or import blocking, PINK1 becomes
338 stabilised in the translocon, phosphorylates latent, pre-existing Ub, which promotes
339 the recruitment of Parkin, triggering the feed-forward mechanism. Ubiquitination of
340 import substrates would provide a ready source of latent Ub for PINK1 to
341 phosphorylate as/when it becomes activated. Interestingly, USP30 has been found to
342 be associated with TOMM20, a *bona fide* substrate of FBXO7 (65), and other
343 translocon assemblies, where basally ubiquitinated translocon import substrates
344 accumulate (39). Consistent with ntc providing the basal ubiquitination in this model,

pS65-Ub that accumulates in *parkin* mutants is both reduced by loss of *ntc* and increased by its overexpression.

While we have shown that *ntc* overexpression is sufficient to induce basal mitophagy, independently of *Pink1/parkin*, and it is able to rescue *parkin* mutant phenotypes, curiously, it is not able to rescue *Pink1* phenotypes. As forced overexpression of *ntc* increases basal ubiquitination, it follows that already high levels of substrate for Pink1 circumvents the need for parkin ubiquitination activity (hence, why *ntc* overexpression can substitute for loss of *parkin*) when stress-induced mitophagy is required. However, despite high levels of latent ubiquitination, this alone is not sufficient to trigger stress-induced mitophagy in the absence of Pink1-mediated phosphorylation (hence, why *ntc* overexpression cannot rescue *Pink1* mutants). These findings further underscore the mechanistic and functional differences between basal and stress-induced mitophagy.

Analysing the potential role of ntc/FBXO7 in mitophagy and the relationship with Pink1/parkin *in vivo* has highlighted the complexity of how different forms of mitophagy may influence tissue homeostasis and relate to organismal phenotypes. As stated before, there are many different forms of mitochondrial quality control and mitophagy, and these perform different functions in cellular remodelling and homeostasis (61, 62). It follows that some forms of mitophagy may dramatically impact neuromuscular homeostasis when disrupted, while others may not. For instance, evidence supports that PINK1/Parkin promote stress-induced mitophagy but are minimally involved in basal mitophagy, and *Drosophila* mutants present multiple robust phenotypes. In contrast, ntc/FBXO7 (and USP30) regulate basal mitophagy and facilitate PINK1/Parkin mitophagy by providing the initiating ubiquitination, yet their mutant phenotypes only loosely resemble those of *Pink1/parkin* mutants.

How do these forms of mitophagy correlate with the mitochondrial/organismal phenotypes? The *Pink1/parkin* phenotypes are consistent with a catastrophic loss of integrity in energy-intensive, mitochondria-rich tissues caused by the lack of a crucial protective measure (induced mitophagy) for a specific circumstance (likely, mitochondrial ‘damage’ arising from a huge metabolic burst). In contrast, while loss of *ntc* causes a partial (but not complete) loss of basal mitophagy, the tissues affected in *Pink1/parkin* mutants appear to be able to cope with loss of this ‘housekeeping’ mitochondrial QC process, consistent with there being partially redundant pathways. Notably, these tissues are still able to mount a stress-induced response via Pink1/parkin as we have observed paraquat-induced accumulation of pS65-Ub in the

382 *ntc* mutant (Figure S5C), reinforcing that stress-induced mitophagy can happen in the
383 absence of ntc. Consequently, *ntc* mutants do not present the same degenerative
384 phenotypes as *Pink1/parkin* mutants and maintain relatively normal mitochondrial
385 function. Hence, it seems likely that the additional *ntc* mutant phenotypes of motor
386 deficits and drastically short lifespan are due to additional functions of ntc/FBXO7,
387 such as regulation of proteasome function and caspase activation, and not mitophagy.
388
389 In summary, we propose a model (Figure 8) in which FBXO7/ntc acts to prime OMM
390 proteins with ubiquitin that is counteracted by USP30. This provides a key regulatory
391 checkpoint in quality control, for instance, during mitochondrial protein import. It is
392 likely that occasional defects in import or protein misfolding may lead to an increase of
393 Ub above a threshold that is sufficient to provoke basal mitophagy. However, when the
394 need arises this population of latent Ub could subsequently be phosphorylated by
395 PINK1 (and amplified by Parkin) to trigger selective degradation upon specific
396 stimulation. Although more studies are required to understand the interplay between
397 FBXO7/ntc, USP30, Pink1 and parkin, this study provides a foundation to further
398 elucidate the interplay between these mechanisms of mitochondrial quality control and
399 reinforces its potential as a therapeutic target.
400

401 **Materials and Methods**

402 ***Drosophila* stocks and procedures**
403 *Drosophila* were raised under standard conditions in a temperature-controlled
404 incubator with a 12h:12h light:dark cycle at 25 °C and 65 % relative humidity, on food
405 consisting of agar, cornmeal, molasses, propionic acid and yeast. *ntc*^{ms771}, *UAS-ntc*
406 and *PBac{WH}CG10855*^{f07259} strains were kindly provided by H. Steller. *park*^{25} mutants
407 and *UAS-parkin*$_{C2}$ (13), *UAS-FBXO7* (27), and *UAS-mito-QC* lines (20) have been
408 previously described. *Pink1*^{B9} mutants (12) were provided by J. Chung (SNU). *UAS-*
409 *Mul1* and *Mul1*^{A6} mutants were kindly provided by Ming Guo. *UAS-USP30* lines were
410 kindly provided by Ugo Mayor. *UAS-USP30* RNAi (NIG-Fly 3016R[II]) was obtained
411 from the NIG-Fly collection. The following strains were obtained from Bloomington
412 *Drosophila* Stock Center (BDSC, RRID:SCR_006457): *w*^{1118} (RRID:BDSC_6326), *da-*
413 *GAL4* (RRID:BDSC_55850), *nSyb-GAL4* (RRID:BDSC_51635), *GMR*-GAL4
414 (RRID:BDSC_1104), *Mef2*-GAL4 (RRID:BDSC_27390), *Act*-GAL4
415 (RRID:BDSC_25374), *Atg8a* [KG07569] *(Atg8a*$^{-/-}$*)* (RRID:BDSC_14639), *UAS-GFP-*
416 *mCherry-Atg8a* (RRID:BDSC_37749) and *Df(3L)Exel6097* (RRID:BDSC_7576). *UAS-*
417 *lacZ* was obtained from FlyORF (RRID: FlyBase_FBst0503118). The following strains

418 were obtained from Vienna Drosophila Research Centre (VDRC): *UAS-LacZ*^{RNAi}
419 (v51446), *UAS-March5* RNAi KK (v105711) and *UAS-March5* RNAi GD(v33309).
420 *UAS-mtx-QC* and *UAS-March5* lines were generated as follows: *mtx-QC* mCherry-
421 GFP was amplified from *UAS-mito-QC* and cloned in-frame with the mitochondrial
422 targeting sequence from hCOX8A into pUAST.attB, and inserted in attP40 and attP16
423 sites; while for *March5* (*CG9855*), full length cDNA was cloned into pUAST vector and
424 transgenesis performed by random insertion. A full description of the genotypes used
425 in this study is shown in Supplementary table 1.
426
427 **Locomotor and lifespan assays**
428 For locomotor assays, climbing (negative geotaxis assay) was assessed as previously
429 described, with minor modifications (13). For lifespan experiments flies were grown
430 under identical conditions at low-density. Progeny were collected under very light
431 anaesthesia and kept in tubes of approximately 20 males each. Flies were transferred
432 every 2-3 days to fresh tubes with normal food for normal lifespan and tubes with 10
433 mM paraquat in a filter paper for the oxidative stress lifespan. The number of dead flies
434 was recorded on each transfer. Percent of survival was calculated at the end of the
435 experiment after correcting for any accidental loss.
436
437 **Histology of adult thoraces**
438 Thoraces were prepared from 5-day-old adult flies and treated as previously described
439 (13). Semi-thin sections were then taken and stained with Toluidine blue, while ultra-
440 thin sections were examined using a FEI Tecnai G2 Spirit 120KV transmission
441 electron-microscope.
442
443 **Light microscopy imaging and scanning electron microscopy of *Drosophila* eye**
444 Light microscopy imaging was assessed using a Nikon motorized SMZ stereo zoom
445 microscope fitted with 1x Apo lens. Extended focus images were then generated using
446 Nikon Elements software, using the same settings for all the genotypes. Flies were
447 anaesthetised with CO2 during the process. Scanning electron microscopy (SEM) was
448 performed according to a standard protocol (66). All animals of a given genotype
449 displayed essentially identical phenotypes and randomly selected representative
450 images are shown. Images were taken using a SEM microscope (Philips XL-20 SEM).
451
452 **Immunohistochemistry and sample preparation**
453 *Drosophila* brains were dissected from 30-day-old flies and immunos-stained with anti-
454 tyrosine hydroxylase (Immunostar Inc. #22491) as described previously (14). Brains

455 were imaged with an Olympus FV1000 confocal with SIM-scanner on a BX61 upright
456 microscope. Tyrosine hydroxylase-positive neurons were counted under blinded
457 conditions. For immunostaining, adult flight muscles were dissected in PBS and fixed
458 in 4% formaldehyde for 30 min, permeabilized in 0.3% Triton X-100 for 30 min, and
459 blocked with 0.3% Triton X-100 plus 1% bovine serum albumin in PBS for 1 h at RT.
460 Tissues were incubated with ATP5A antibody (Abcam Cat# ab14748,
461 RRID:AB_301447; 1:500), diluted in 0.3% Triton X-100 plus 1% bovine serum albumin
462 in PBS overnight at 4°C, then rinsed 3 times 10 min with 0.3% Triton X-100 in PBS,
463 and incubated with the appropriate fluorescent secondary antibodies overnight at 4°C.
464 The tissues were washed 3 times in PBS and mounted on slides using ProLong
465 Diamond Antifade mounting medium (Thermo Fisher Scientific) and image next day.
466 For mitolysosome analysis of *mito-QC* and *mtx-QC*, tissues were dissected and
467 treated as previously described (20).
468
469 **Mitochondrial morphology in larval brain**
470 Third instar larvae overexpressing *UAS-mitoGFP* with the pan-neuronal driver nSyb-
471 GAL4 were dissected in PBS and fixed in 4% formaldehyde for 30 min. The tissues
472 were washed 3 times in PBS and mounted on slides using ProLong Diamond Antifade
473 mounting medium (Thermo Fisher Scientific) and image next day in a Zeiss LSM880
474 confocal microscope (63x / 1.4NA).
475
476 **ATP levels**
477 The ATP assay was performed as described previously (67). Briefly, five male flies of
478 the indicated age for each genotype were homogenized in 100 μL 6M guanidine-
479 Tris/EDTA extraction buffer and subjected to rapid freezing in liquid nitrogen.
480 Homogenates were diluted 1/100 with the extraction buffer and mixed with the
481 luminescent solution (CellTiter-Glo Luminescent Cell Viability Assay (Promega,
482 RRID:SCR_006724)). Luminescence was measured with a SpectraMax Gemini XPS
483 luminometer (Molecular Devices). The average luminescent signal from technical
484 triplicates was expressed relative to protein levels, quantified using the DC Protein
485 Assay kit (Bio-Rad Laboratories, RRID:SCR_008426). Data from 2-4 independent
486 experiments were averaged and the luminescence expressed as a percentage of the
487 control.
488
489 **Respirometry**
490 Mitochondrial respiration was assayed at 30 °C by high-resolution respirometry using
491 an Oxygraph-2k high-resolution respirometer (OROBOROS Instruments) using a

492 chamber volume set to 2 mL. Calibration with the air-saturated medium was performed
493 daily. Data acquisition and analysis were carried out using Datlab software
494 (OROBOROS Instruments). Five flies per genotype were homogenised in Respiration
495 Buffer [120 mM sucrose, 50 mM KCl, 20 mM Tris–HCl, 4 mM KH_2PO_4, 2 mM $MgCl_2$,
496 and 1 mM EGTA, 1 g L^{-1} fatty acid-free BSA, pH 7.2]. For coupled (state 3) assays,
497 complex I-linked respiration was measured at saturating concentrations of malate
498 (2 mM), glutamate (10 mM), L-proline (10 mM) and adenosine diphosphate (ADP,
499 2.5 mM). Complex II-linked respiration was assayed in Respiration Buffer
500 supplemented with 0.15 μM rotenone, 10 mM succinate and 2.5 mM ADP. Respiration
501 was expressed as oxygen consumed per fly. Flies' weight was equal in all genotypes
502 tested.
503
504 **Image analysis and quantification of mitolysosomes**
505 Analysis of mitolysosomes was done as previously described (20). Briefly, spinning
506 disk microscopy–generated images from dissected larval brains or adult thoraces were
507 processed using Imaris (version 9.0.2) analysis software (BitPlane;
508 RRID:SCR_007370) to identify and count individual red-only puncta. The GFP and
509 mCherry signals were adjusted to reduce background noise and retain only the distinct
510 mitochondria network and red puncta, respectively. A surface rendered 3D structure
511 corresponding to the mitochondria network was generated using the GFP signal. This
512 volume was subtracted from the red channel to retain the mCherry signal that did not
513 colocalize with the GFP-labelled mitochondria network. The mitolysosomes puncta
514 were selected according to their intensity and an estimated size of 0.5 μm diameter,
515 previously measured with Imaris. Additionally, the puncta were filtered with a minimum
516 size cut off of 0.2 μm diameter. The remaining puncta were counted as the number of
517 mitolysosomes. Larval CNS soma were analysed individually where discrete cells
518 could be distinguished. The mean number of mitolysosomes per cell was calculated
519 per animal. Data points in the quantification charts show mean mitolysosomes per cell
520 for individual animals, where $n \geq 6$ animals for each condition.
521
522 **Analysis and quantification of autolysosomes using the GFP-mCherry-Atg8a**
523 **traffic light reporter.**
524 Third instar larval brains were dissected in phosphate buffered saline (PBS) and fixed
525 with 4 % formaldehyde (FA) pH 7 (Thermo Scientific)/PBS for 20 minutes at room
526 temperature. Samples were then washed in PBS followed by water to remove salts.
527 ProLong antifade mounting media (Thermo Scientific) was used to mount the samples
528 and imaged the day after. Confocal images, acquired with a Zeiss LSM880 microscope

529 with the 63x/1.4 NA oil, were processed using FIJI (Image J). The quantification of
530 autolysosomes was performed using FIJI (Image J) with the 3D Objects Counter
531 Plugin. An area of interest was selected by choosing 6-10 cells per image. The
532 threshold was based on matching the mask with the fluorescence. All puncta larger
533 than 0.049 μm^3 was considered an autolysosome. Data points in the quantification
534 charts show mean mitolysosomes per cell for individual animals, where $n \geq 3$ animals
535 for each condition.
536
537 **Mitochondrial enrichment by differential centrifugation**
538 All steps were performed on ice or at 4 °C. For immunoblotting analysis and
539 biochemical fractionation from small numbers of flies (10-30), a modified mitochondrial
540 enrichment procedure was performed. Flies were prepared either fresh or after flash-
541 freezing in liquid nitrogen, with all direct comparisons performed with flies that were
542 prepared in the same manner. Flies were transferred into a Dounce homogeniser
543 containing 700 µL Solution A (70 mM sucrose, 20 mM HEPES pH 7.6, 220 mM
544 mannitol, 1 mM EDTA) containing cOmplete protease inhibitors (Roche) and
545 PhosSTOP phosphatase inhibitors (Roche), and manually homogenised with 50
546 strokes of a pestle. The homogenate was transferred to an Eppendorf tube, a further
547 500 µl of Solution A was added to the homogeniser and the sample was homogenised
548 with a further 10 strokes. The homogenates were pooled and incubated for 30 minutes,
549 then centrifuged for 5 minutes at 800 x g. The supernatant (containing mitochondria)
550 was transferred to a new tube and clarified twice by centrifugation for 5 minutes at
551 1,000 x g. The clarified supernatant was then centrifuged for 10 minutes at 10,000 x g
552 and the post-mitochondrial supernatant was discarded and the pellet retained for
553 analysis. The mitochondrial pellet was washed once in Solution A containing only
554 protease inhibitors, and then once in Solution A without inhibitors. The washed
555 mitochondrial pellet was resuspended in 50 to 200 µL Sucrose Storage Buffer, the
556 protein content determined by BCA assay (Thermo Pierce), and stored at -80 °C until
557 needed.
558
559 **Antibodies and dyes**
560 The following mouse antibodies were used for immunoblotting (WB) in this study:
561 ATP5A (Abcam, ab14748, 1:10000), actin (Millipore, MAB1501, 1:5000), Ubiquitin
562 (clone P4D1, Cell Signalling Technology, 3936, 1:1000), Ubiquitin (clone FK2, MBL,
563 D058-3, 1:1000). The following rabbit antibodies were used in this study: pS65-Ub
564 (Cell Signalling Technologies, 62802S, 1:1000), Marf ((16), 1:1000), GABARAP/Atg8a
565 (Abcam ab109364, 1:1000), ref(2)P/p62 (Abcam ab178440, 1:1000). The following

566 secondary antibodies were used: sheep anti-mouse (HRP-conjugated, GE Healthcare,
567 NXA931V, 1:10000), donkey anti-rabbit (HRP-conjugated, GE Healthcare, NA934V,
568 1:10000).
569
570 **Whole-animal lysis and immunoblotting**
571 For the analysis of whole cell lysates by immunoblot, 180 µL cold RIPA buffer (150
572 mM NaCl, 1% (v/v) NP-40, 0.5 % (w/v) sodium deoxycholate, 0.1% (w/v) SDS, 50 mM
573 Tris pH 7.4), supplemented with cOmplete protease inhibitors, was added to 2 mL
574 tubes containing 1.4 mm ceramic beads (Fisherbrand 15555799). Animals (5 to 20 per
575 replicate) were harvested and stored on ice or flash-frozen in liquid N_2, with all direct
576 comparisons performed with flies that were harvested in the same manner. The flies
577 were added to the tubes containing RIPA buffer and lysed using a Minilys homogeniser
578 (Bertin Instruments) with the following settings: maximum speed, 10 seconds on, 10
579 seconds on ice, for a total of three cycles. After lysis, samples were returned to ice for
580 10 minutes then centrifuged 5 minutes at 21,000 x g, 4 °C. 90 µL supernatant was
581 transferred to a fresh Eppendorf tube and centrifuged a further 10 minutes at 21,000 x
582 g. 50 µL supernatant was then transferred to a fresh Eppendorf tube and the protein
583 content determined by BCA assay as above. 30 µg total protein was then diluted in
584 Laemmli Sample Buffer (Bio-Rad, 1610747) and analysed by SDS-PAGE using Mini-
585 PROTEAN TGX Gels 4-20% (Bio-Rad, 4561093). For the analysis of mitochondria-
586 enriched fractions, 30 µg mitochondrial protein was aliquoted into a tube, centrifuged
587 10 minutes at 16,000 x g, the supernatant removed and the pellet resuspended in
588 Laemmli Sample Buffer (Bio-Rad, 1610747) to SDS-PAGE analysis as above. Gels
589 were transferred onto pre-cut and soaked PVDF membranes (1704156, BioRad) using
590 the BioRad Transblot Turbo transfer system, and blots were immediately stained with
591 No-Stain™ Protein Labeling Reagent (Invitrogen, A44449) where indicated, according
592 to the manufacturer's instructions. Fluorescence intensity was measured using a
593 BioRad Chemidoc MP using the IR680 setting. Blots were then washed by gentle
594 shaking 3 times for 5 minutes in PBS containing 0.1% (v/v) Tween-20 (PBST), and
595 blocked by incubation with PBST containing 3 % (w/v) BSA for 1 hour. Blots were
596 washed a further 3 times as above then incubated at 4 °C overnight with primary
597 antibodies in PBST containing 3 % (w/v) BSA. A further 3 washes were performed then
598 the blots were incubated for one hour in secondary antibodies made up in PBST
599 containing 3 % (w/v) BSA. Blots were then washed twice in PBST and once in PBS
600 prior to incubation with ECL Prime western blotting System (Cytiva, RPN2232). Blots
601 were imaged using the BioRad Chemidoc MP using exposure settings to minimise
602 overexposure. Image analysis was performed using FIJI (Image J) and images were

603 exported as TIFF files for publication. For paraquat treatment, flies were maintained in
604 tubes (10-20 flies per replicate) containing 6 semi-circular pieces of filter paper (90 mm
605 diameter, Cat#1001-090) saturated with 5% (w/v) sucrose solution containing 10 mM
606 paraquat. Sucrose-only starvation experiments were performed as above, with the
607 omission of paraquat. After 3 days, the flies were anaesthetised with mild CO_2 and live
608 flies only were harvested and process for immunoblotting as described above.
609

610 **ARPE-19-MQC cells**

611 ARPE-19-MQC-FIS1 cells were used to assess mitophagy in a human cell model.
612 Briefly, cells were transfected in reverse with RNAiMax (13778075, Thermo Fisher
613 Scientific) and non-targeting control siRNA (ON-TARGETplus Non-targeting Control
614 Pool, D-001810-10-20, Horizon Discovery) or FBXO7 siRNA (ON-TARGETplus
615 Human FBXO7 siRNA, L-013606-00-0010, Horizon Discovery). After 48h knockdown
616 cells were seeded into and ibidi dish (IB-81156) Thistle Scientific Ltd), and after 72h
617 cells were imaged live by a spinning disk microscope and generated images were
618 processed using Imaris as previously described.
619

620 **Statistical analysis**

621 Data are reported as mean ± SEM or mean ± 95% CI as indicated in figure legends,
622 and the n numbers of distinct biological replicates are shown in each graph. For
623 statistical analyses of lifespan experiments, a log rank (Mantel-Cox) test was used. For
624 behavioural analyses, a Kruskal-Wallis nonparametric test with Dunn's post-hoc test
625 correction for multiple comparisons was used. Where multiple groups were compared,
626 statistical significance was calculated by one-way ANOVA with Bonferroni post-hoc
627 test correction for multiple samples. This test was applied to dopaminergic neuron
628 analysis and mitophagy where more than two groups were compared. For Ub and
629 pS65-Ub abundance a one-way ANOVA with Dunnett's correction for multiple
630 comparisons was used. When only two groups were compared a Welch's *t* test was
631 used. The absence of statistical analysis in between any group reflects "no statistical
632 significance". All the samples were collected and processed simultaneously and
633 therefore no randomization was appropriate. Unless otherwise indicated, all the
634 acquisition of images and analysis was done in blind conditions. Statistical analyses
635 were performed using GraphPad Prism 9 software (GraphPad Prism,
636 RRID:SCR_002798). Statistical significance was represented in all cases as follows: *
637 $P < 0.05$, ** $P < 0.01$, *** $P < 0.001$ and **** $P < 0.0001$.
638

Data Availability

All data needed to evaluate the conclusions in the paper are present in the paper and/or the Supplementary Materials. This study includes no data deposited in external repositories. Additional data related to this paper may be requested from the authors.

Acknowledgements

We kindly thank Herman Steller for generously sharing the ntc lines, Ugo Mayor for the USP30 overexpression lines and Ian Ganley for the ARPE-19-MQC cells. We thank Roberta Tufi for performing the ATP assay, Wing Hei Au and Federica De Lazzari for comments and edits on the manuscript, and all the members of the Whitworth's lab for discussions.

Funding

This work is supported by MRC core funding (MC_UU_00028/6). A.M. is funded by the Basque Government Postdoctoral Fellowship. Stocks were obtained from the Bloomington *Drosophila* Stock Center which is supported by grant NIH P40OD018537.

Author contributions

A.S.M. conceived the project, designed the experiments, performed experimental work, analysed data, wrote the original draft, revised and edited the manuscript.

A.M. conceived parts of the project, designed and performed some experimental work, analysed data and revised and edited the manuscript.

A.J.W. conceived and supervised the project, wrote the original draft, revised and edited the manuscript.

Authors ORCIDs

Alvaro Sanchez-Martinez https://orcid.org/0000-0002-2728-6251

Aitor Martinez https://orcid.org/0000-0003-1648-9448

Alexander J Whitworth https://orcid.org/0000-0002-1154-6629

Competing interests

The authors declare that they have no competing interests.

672 **References**

673

674 1. Yamano K, Youle RJ. PINK1 is degraded through the N-end rule pathway.
675 Autophagy. 2013;9(11):1758-69.
676 2. Okatsu K, Kimura M, Oka T, Tanaka K, Matsuda N. Unconventional PINK1
677 localization to the outer membrane of depolarized mitochondria drives Parkin
678 recruitment. J Cell Sci. 2015;128(5):964-78.
679 3. Okatsu K, Koyano F, Kimura M, Kosako H, Saeki Y, Tanaka K, et al.
680 Phosphorylated ubiquitin chain is the genuine Parkin receptor. J Cell Biol.
681 2015;209(1):111-28.
682 4. Gladkova C, Maslen SL, Skehel JM, Komander D. Mechanism of parkin
683 activation by PINK1. Nature. 2018;559(7714):410-4.
684 5. Sauve V, Sung G, Soya N, Kozlov G, Blaimschein N, Miotto LS, et al.
685 Mechanism of parkin activation by phosphorylation. Nature structural &
686 molecular biology. 2018;25(7):623-30.
687 6. Ordureau A, Sarraf SA, Duda DM, Heo JM, Jedrychowski MP, Sviderskiy VO, et
688 al. Quantitative proteomics reveal a feedforward mechanism for mitochondrial
689 PARKIN translocation and ubiquitin chain synthesis. Mol Cell. 2014;56(3):360-
690 75.
691 7. Bingol B, Sheng M. Mechanisms of mitophagy: PINK1, Parkin, USP30 and
692 beyond. Free Radic Biol Med. 2016;100:210-22.
693 8. Lazarou M, Sliter DA, Kane LA, Sarraf SA, Wang C, Burman JL, et al. The
694 ubiquitin kinase PINK1 recruits autophagy receptors to induce mitophagy.
695 Nature. 2015;524(7565):309-14.
696 9. Yamano K, Kikuchi R, Kojima W, Hayashida R, Koyano F, Kawawaki J, et al.
697 Critical role of mitochondrial ubiquitination and the OPTN-ATG9A axis in
698 mitophagy. J Cell Biol. 2020;219(9).

699 10. Pickrell AM, Youle RJ. The roles of PINK1, parkin, and mitochondrial fidelity in
700 Parkinson's disease. Neuron. 2015;85(2):257-73.
701 11. Clark IE, Dodson MW, Jiang C, Cao JH, Huh JR, Seol JH, et al. Drosophila
702 pink1 is required for mitochondrial function and interacts genetically with parkin.
703 Nature. 2006;441(7097):1162-6.
704 12. Park J, Lee SB, Lee S, Kim Y, Song S, Kim S, et al. Mitochondrial dysfunction in
705 Drosophila PINK1 mutants is complemented by parkin. Nature.
706 2006;441(7097):1157-61.
707 13. Greene JC, Whitworth AJ, Kuo I, Andrews LA, Feany MB, Pallanck LJ.
708 Mitochondrial pathology and apoptotic muscle degeneration in Drosophila parkin
709 mutants. Proceedings of the National Academy of Sciences of the United States
710 of America. 2003;100(7):4078-83.
711 14. Whitworth AJ, Theodore DA, Greene JC, Benes H, Wes PD, Pallanck LJ.
712 Increased glutathione S-transferase activity rescues dopaminergic neuron loss in
713 a Drosophila model of Parkinson's disease. Proc Natl Acad Sci U S A.
714 2005;102(22):8024-9.
715 15. Poole AC, Thomas RE, Andrews LA, McBride HM, Whitworth AJ, Pallanck LJ.
716 The PINK1/Parkin pathway regulates mitochondrial morphology. Proceedings of
717 the National Academy of Sciences of the United States of America.
718 2008;105(5):1638-43.
719 16. Ziviani E, Tao RN, Whitworth AJ. Drosophila parkin requires PINK1 for
720 mitochondrial translocation and ubiquitinates mitofusin. Proceedings of the
721 National Academy of Sciences of the United States of America.
722 2010;107(11):5018-23.
723 17. Vincow ES, Merrihew G, Thomas RE, Shulman NJ, Beyer RP, MacCoss MJ, et
724 al. The PINK1-Parkin pathway promotes both mitophagy and selective
725 respiratory chain turnover in vivo. Proceedings of the National Academy of
726 Sciences of the United States of America. 2013;110(16):6400-5.

727 18. Cornelissen T, Verstreken P, Vandenberghe W. Imaging mitophagy in the fruit
728 fly. Autophagy. 2018;14(9):1656-7.
729 19. Kim YY, Um JH, Yoon JH, Kim H, Lee DY, Lee YJ, et al. Assessment of
730 mitophagy in mt-Keima Drosophila revealed an essential role of the PINK1-
731 Parkin pathway in mitophagy induction in vivo. FASEB J. 2019;33(9):9742-51.
732 20. Lee JJ, Sanchez-Martinez A, Martinez Zarate A, Beninca C, Mayor U, Clague
733 MJ, et al. Basal mitophagy is widespread in Drosophila but minimally affected by
734 loss of Pink1 or parkin. J Cell Biol. 2018;217(5):1613-22.
735 21. McWilliams TG, Prescott AR, Montava-Garriga L, Ball G, Singh F, Barini E, et al.
736 Basal Mitophagy Occurs Independently of PINK1 in Mouse Tissues of High
737 Metabolic Demand. Cell metabolism. 2018;27(2):439-49 e5.
738 22. Di Fonzo A, Dekker MC, Montagna P, Baruzzi A, Yonova EH, Correia Guedes L,
739 et al. FBXO7 mutations cause autosomal recessive, early-onset parkinsonian-
740 pyramidal syndrome. Neurology. 2009;72(3):240-5.
741 23. Zhou ZD, Lee JCT, Tan EK. Pathophysiological mechanisms linking F-box only
742 protein 7 (FBXO7) and Parkinson's disease (PD). Mutat Res Rev Mutat Res.
743 2018;778:72-8.
744 24. Skowyra D, Craig KL, Tyers M, Elledge SJ, Harper JW. F-box proteins are
745 receptors that recruit phosphorylated substrates to the SCF ubiquitin-ligase
746 complex. Cell. 1997;91(2):209-19.
747 25. Hsu JM, Lee YC, Yu CT, Huang CY. Fbx7 functions in the SCF complex
748 regulating Cdk1-cyclin B-phosphorylated hepatoma up-regulated protein (HURP)
749 proteolysis by a proline-rich region. J Biol Chem. 2004;279(31):32592-602.
750 26. Kirk R, Laman H, Knowles PP, Murray-Rust J, Lomonosov M, Meziane el K, et
751 al. Structure of a conserved dimerization domain within the F-box protein Fbxo7
752 and the PI31 proteasome inhibitor. The Journal of biological chemistry.
753 2008;283(32):22325-35.

754 27. Burchell VS, Nelson DE, Sanchez-Martinez A, Delgado-Camprubi M, Ivatt RM,
755 Pogson JH, et al. The Parkinson's disease-linked proteins Fbxo7 and Parkin
756 interact to mediate mitophagy. Nat Neurosci. 2013;16(9):1257-65.
757 28. Bader M, Arama E, Steller H. A novel F-box protein is required for caspase
758 activation during cellular remodeling in Drosophila. Development.
759 2010;137(10):1679-88.
760 29. Bader M, Benjamin S, Wapinski OL, Smith DM, Goldberg AL, Steller H. A
761 conserved F box regulatory complex controls proteasome activity in Drosophila.
762 Cell. 2011;145(3):371-82.
763 30. Song S, Jang S, Park J, Bang S, Choi S, Kwon KY, et al. Characterization of
764 PINK1 (PTEN-induced putative kinase 1) mutations associated with Parkinson
765 disease in mammalian cells and Drosophila. J Biol Chem. 2013;288(8):5660-72.
766 31. Whitworth AJ, Lee JR, Ho VM, Flick R, Chowdhury R, McQuibban GA.
767 Rhomboid-7 and HtrA2/Omi act in a common pathway with the Parkinson's
768 disease factors Pink1 and Parkin. Dis Model Mech. 2008;1(2-3):168-74;
769 discussion 73.
770 32. Riparbelli MG, Callaini G. The Drosophila parkin homologue is required for
771 normal mitochondrial dynamics during spermiogenesis. Dev Biol.
772 2007;303(1):108-20.
773 33. Meulener M, Whitworth AJ, Armstrong-Gold CE, Rizzu P, Heutink P, Wes PD, et
774 al. Drosophila DJ-1 mutants are selectively sensitive to environmental toxins
775 associated with Parkinson's disease. Curr Biol. 2005;15(17):1572-7.
776 34. Malik BR, Godena VK, Whitworth AJ. VPS35 pathogenic mutations confer no
777 dominant toxicity but partial loss of function in Drosophila and genetically interact
778 with parkin. Hum Mol Genet. 2015;24(21):6106-17.
779 35. Allen GF, Toth R, James J, Ganley IG. Loss of iron triggers PINK1/Parkin-
780 independent mitophagy. EMBO Rep. 2013;14(12):1127-35.

781 36. Shen JL, Fortier TM, Wang R, Baehrecke EH. Vps13D functions in a Pink1-
782 dependent and Parkin-independent mitophagy pathway. J Cell Biol.
783 2021;220(11).
784 37. Montava-Garriga L, Singh F, Ball G, Ganley IG. Semi-automated quantitation of
785 mitophagy in cells and tissues. Mech Ageing Dev. 2020;185:111196.
786 38. Marcassa E, Kallinos A, Jardine J, Rusilowicz-Jones EV, Martinez A, Kuehl S, et
787 al. Dual role of USP30 in controlling basal pexophagy and mitophagy. EMBO
788 Rep. 2018;19(7).
789 39. Ordureau A, Paulo JA, Zhang J, An H, Swatek KN, Cannon JR, et al. Global
790 Landscape and Dynamics of Parkin and USP30-Dependent Ubiquitylomes in
791 iNeurons during Mitophagic Signaling. Mol Cell. 2020;77(5):1124-42 e10.
792 40. Rusilowicz-Jones EV, Jardine J, Kallinos A, Pinto-Fernandez A, Guenther F,
793 Giurrandino M, et al. USP30 sets a trigger threshold for PINK1-PARKIN
794 amplification of mitochondrial ubiquitylation. Life Sci Alliance. 2020;3(8).
795 41. Bingol B, Tea JS, Phu L, Reichelt M, Bakalarski CE, Song Q, et al. The
796 mitochondrial deubiquitinase USP30 opposes parkin-mediated mitophagy.
797 Nature. 2014;510(7505):370-5.
798 42. Phu L, Rose CM, Tea JS, Wall CE, Verschueren E, Cheung TK, et al. Dynamic
799 Regulation of Mitochondrial Import by the Ubiquitin System. Mol Cell.
800 2020;77(5):1107-23 e10.
801 43. Yun J, Puri R, Yang H, Lizzio MA, Wu C, Sheng ZH, et al. MUL1 acts in parallel
802 to the PINK1/parkin pathway in regulating mitofusin and compensates for loss of
803 PINK1/parkin. Elife. 2014;3:e01958.
804 44. Rojansky R, Cha MY, Chan DC. Elimination of paternal mitochondria in mouse
805 embryos occurs through autophagic degradation dependent on PARKIN and
806 MUL1. Elife. 2016;5.
807 45. Zheng J, Chen X, Liu Q, Zhong G, Zhuang M. Ubiquitin ligase MARCH5
808 localizes to peroxisomes to regulate pexophagy. J Cell Biol. 2022;221(1).

809 46. Chen Z, Liu L, Cheng Q, Li Y, Wu H, Zhang W, et al. Mitochondrial E3 ligase
810 MARCH5 regulates FUNDC1 to fine-tune hypoxic mitophagy. EMBO Rep.
811 2017;18(3):495-509.
812 47. Koyano F, Yamano K, Kosako H, Kimura Y, Kimura M, Fujiki Y, et al. Parkin-
813 mediated ubiquitylation redistributes MITOL/March5 from mitochondria to
814 peroxisomes. EMBO Rep. 2019;20(12):e47728.
815 48. Liang JR, Martinez A, Lane JD, Mayor U, Clague MJ, Urbe S. USP30
816 deubiquitylates mitochondrial Parkin substrates and restricts apoptotic cell
817 death. EMBO Rep. 2015;16(5):618-27.
818 49. Pan W, Wang Y, Bai X, Yin Y, Dai L, Zhou H, et al. Deubiquitinating enzyme
819 USP30 negatively regulates mitophagy and accelerates myocardial cell
820 senescence through antagonism of Parkin. Cell Death Discov. 2021;7(1):187.
821 50. Lazarou M, McKenzie M, Ohtake A, Thorburn DR, Ryan MT. Analysis of the
822 assembly profiles for mitochondrial- and nuclear-DNA-encoded subunits into
823 complex I. Mol Cell Biol. 2007;27(12):4228-37.
824 51. Nguyen TN, Padman BS, Usher J, Oorschot V, Ramm G, Lazarou M. Atg8
825 family LC3/GABARAP proteins are crucial for autophagosome-lysosome fusion
826 but not autophagosome formation during PINK1/Parkin mitophagy and
827 starvation. J Cell Biol. 2016;215(6):857-74.
828 52. Jipa A, Vedelek V, Merenyi Z, Urmosi A, Takats S, Kovacs AL, et al. Analysis of
829 Drosophila Atg8 proteins reveals multiple lipidation-independent roles.
830 Autophagy. 2021;17(9):2565-75.
831 53. Yoshii SR, Mizushima N. Monitoring and Measuring Autophagy. Int J Mol Sci.
832 2017;18(9).
833 54. Lorincz P, Mauvezin C, Juhasz G. Exploring Autophagy in Drosophila. Cells.
834 2017;6(3).
835 55. Mauvezin C, Ayala C, Braden CR, Kim J, Neufeld TP. Assays to monitor
836 autophagy in Drosophila. Methods. 2014;68(1):134-9.

837 56. Nagy P, Karpati M, Varga A, Pircs K, Venkei Z, Takats S, et al. Atg17/FIP200
838 localizes to perilysosomal Ref(2)P aggregates and promotes autophagy by
839 activation of Atg1 in Drosophila. Autophagy. 2014;10(3):453-67.
840 57. Low P, Varga A, Pircs K, Nagy P, Szatmari Z, Sass M, et al. Impaired
841 proteasomal degradation enhances autophagy via hypoxia signaling in
842 Drosophila. BMC Cell Biol. 2013;14:29.
843 58. Gersch M, Gladkova C, Schubert AF, Michel MA, Maslen S, Komander D.
844 Mechanism and regulation of the Lys6-selective deubiquitinase USP30. Nature
845 structural & molecular biology. 2017;24(11):920-30.
846 59. Usher JL, Sanchez-Martinez A, Terriente-Felix A, Chen PL, Lee JJ, Chen CH, et
847 al. Parkin drives pS65-Ub turnover independently of canonical autophagy in
848 Drosophila. EMBO Rep. 2022:e202153552.
849 60. Zhou ZD, Xie SP, Sathiyamoorthy S, Saw WT, Sing TY, Ng SH, et al. F-box
850 protein 7 mutations promote protein aggregation in mitochondria and inhibit
851 mitophagy. Hum Mol Genet. 2015;24(22):6314-30.
852 61. Ashrafi G, Schwarz TL. The pathways of mitophagy for quality control and
853 clearance of mitochondria. Cell Death Differ. 2013;20(1):31-42.
854 62. Pickles S, Vigie P, Youle RJ. Mitophagy and Quality Control Mechanisms in
855 Mitochondrial Maintenance. Curr Biol. 2018;28(4):R170-R85.
856 63. Cunningham CN, Baughman JM, Phu L, Tea JS, Yu C, Coons M, et al. USP30
857 and parkin homeostatically regulate atypical ubiquitin chains on mitochondria.
858 Nature cell biology. 2015;17(2):160-9.
859 64. Ordureau A, Heo JM, Duda DM, Paulo JA, Olszewski JL, Yanishevski D, et al.
860 Defining roles of PARKIN and ubiquitin phosphorylation by PINK1 in
861 mitochondrial quality control using a ubiquitin replacement strategy. Proceedings
862 of the National Academy of Sciences of the United States of America.
863 2015;112(21):6637-42.

65. Teixeira FR, Randle SJ, Patel SP, Mevissen TE, Zenkeviciute G, Koide T, et al. Gsk3beta and Tomm20 are substrates of the SCFFbxo7/PARK15 ubiquitin ligase associated with Parkinson's disease. Biochem J. 2016;473(20):3563-80.
66. Sullivan WA, M. ; Hawley, R. S. Drosophila protocols. Cold Spring Harbor Laboratory Press. 2000.
67. Pogson JH, Ivatt RM, Sanchez-Martinez A, Tufi R, Wilson E, Mortiboys H, et al. The Complex I Subunit NDUFA10 Selectively Rescues Drosophila pink1 Mutants through a Mechanism Independent of Mitophagy. PLoS genetics. 2014;10(11):e1004815.

875 **Figure Legends**

876

877 **Figure 1. ntc overexpression is able to rescue *parkin* but not *Pink1* mutants.**
878 (**A**) Climbing ability of 2-day-old control and *parkin* mutants alone or with transgenic
879 expression of *ntc* with the ubiquitous driver *da*-GAL4. Chart show mean ± 95% CI and
880 n values. Kruskal-Wallis nonparametric test with Dunn's post-hoc test correction for
881 multiple comparisons; **** $P < 0.0001$. (**B**) Quantification of dopaminergic neurons
882 (PPL1 cluster) in 30-day-old control and *parkin* mutants alone or with transgenic
883 expression of *ntc* with the ubiquitous driver *da*-GAL4. Data represented as mean ±
884 SEM; n shown in chart. One-way ANOVA with Bonferroni post-hoc test correction; ****
885 $P < 0.0001$. (**C**) Toluidine blue staining, and (**D**) transmission electron microscopy
886 (TEM) analysis of thoraces from 2-day-old control and *parkin* mutant alone or with
887 transgenic expression of *ntc* with the ubiquitous driver *da*-GAL4. Scale bars; top = 200
888 µm, middle = 10 µm, bottom = 2 µm. (**E**) Immunoblot analysis from whole fly lysates of
889 Marf steady state levels from 2-day-old control and *parkin* mutants alone or with
890 transgenic expression of *ntc* with the ubiquitous driver *da*-GAL4. Numbers below blots
891 indicated the mean ± SD of Marf levels normalised to ATP5A loading control across 3
892 replicate experiments. (**F**) Climbing and (**G**) flight ability of 2-day-old control and *Pink1*
893 mutants alone or with transgenic expression of *ntc* with the ubiquitous driver *da*-GAL4.
894 Chart show mean ± 95% CI; n shown in chart. Kruskal-Wallis nonparametric test with
895 Dunn's post-hoc test correction for multiple comparisons; **** $P < 0.0001$. (**H**)
896 Immunoblot analysis from whole fly lysates of Marf steady state levels from 2-day-old
897 control and *Pink1* mutants alone or with transgenic expression of *ntc* with the
898 ubiquitous driver *da*-GAL4. Numbers below blots indicated the mean ± SD of Marf
899 levels normalised to ATP5A loading control across 3 replicate experiments. (**I**) Analysis
900 of the compound eye by (top panels) light microscopy or (middle and bottom panels)
901 scanning electron microscopy (SEM) of 2-day-old control, overexpression of ntc, Pink1
902 or both combine using the *GMR*-GAL4 driver. Scale bars; top and middle = 100 µm,
903 bottom = 50 µm.

904

905 **Figure 2. Loss of ntc has motor and lifespan deficits, no gross effect on**
906 **mitochondria but increased sensitivity to oxidative stress.**
907 Analysis of (**A**) climbing and (**B**) flight abilities of 2-day-old control and *ntc* mutants
908 alone or with transgenic expression of *ntc* with the ubiquitous driver *da*-GAL4. Chart
909 show mean ± 95% CI and n values. Kruskal-Wallis nonparametric test with Dunn's
910 post-hoc test correction for multiple comparisons; ** $P < 0.01$, *** $P < 0.001$, **** $P <$
911 0.0001. (**C**) Lifespan assay of control and *ntc* mutants alone or with transgenic

912 expression of *ntc* with the ubiquitous driver *da*-GAL4; n shown in chart. Log rank
913 (Mantel-Cox) test; **** $P < 0.0001$. (**D**) Quantification of dopaminergic neurons (PPL1
914 cluster) in 10-day-old control and *ntc* mutants alone. Data represented as mean ±
915 SEM; n shown in chart. One-way ANOVA with Bonferroni post-hoc test correction. (**E**)
916 (Top panel) Immunohistochemistry with anti-ATP5A staining and (bottom panel)
917 transmission electron microscopy of 2-day-old adult thoraces from control and *ntc*
918 mutants. Scale bars; top = 10 μm, bottom = 2 μm. (**F**) Mitochondrial morphology in
919 motoneurons from the ventral nerve cord of third instar larvae in control and *ntc*
920 mutants, overexpressing mito-GFP with the pan-neuronal driver *nSyb*-GAL4. Scale
921 bars = 10 μm. (**G**) Oxygen consumption rate from complex I and complex II of 2-day-
922 old control and *ntc* mutants. Data represented as mean ± SEM; n shown in chart. One-
923 way ANOVA with Bonferroni post-hoc test correction. (**H**) ATP levels of 2-day-old
924 control and *ntc* mutants alone or with transgenic expression of *ntc* with the ubiquitous
925 driver *da*-GAL4. Data represented as mean ± SEM; n shown in chart. One-way ANOVA
926 with Bonferroni post-hoc test correction; * $P < 0.05$, ** $P < 0.01$. (**I**) Lifespan assay of
927 control and *ntc* mutants treated with 10 μM paraquat. n shown in chart. Log rank
928 (Mantel-Cox) test; **** $P < 0.0001$.
929
930 **Figure 3. ntc affects basal mitophagy and counteracts USP30.**
931 (**A**, **B**) Confocal microscopy analysis of the *mito-QC* reporter in larval CNS of control
932 and *ntc* mutant alone or with transgenic expression of *ntc* with the pan-neuronal driver
933 *nSyb*-GAL4. Mitolysosomes are evident as GFP-negative/mCherry-positive (red-only)
934 puncta. n shown in chart. One-way ANOVA with Bonferroni post-hoc test correction;
935 ** $P < 0.01$. Scale bars = 10 μm. (**C**, **D**) Confocal microscopy analysis of the *mito-QC*
936 reporter in larval CNS of control and transgenic expression of *ntc* with the pan-neuronal
937 driver *nSyb*-GAL4. Mitolysosomes are evident as GFP-negative/mCherry-positive
938 (red-only) puncta. n shown in chart. One-way ANOVA with Bonferroni post-hoc test
939 correction; *** $P < 0.001$. Scale bars = 10 μm. (**E**, **F**) Confocal microscopy analysis of
940 the *mito-QC* reporter in larval CNS of control and knockdown of USP30 with the pan-
941 neuronal driver *nSyb*-GAL4 alone or in combination with *ntc* mutant. Mitolysosomes
942 are evident as GFP-negative/mCherry-positive (red-only) puncta. n shown in chart.
943 One-way ANOVA with Bonferroni post-hoc test correction; * $P < 0.05$, *** $P < 0.001$.
944 Scale bars = 10 μm. (**G**) Climbing ability of 10-day-old flies overexpressing USP30
945 alone or in combination with ntc or parkin with the ubiquitous driver *Act*-GAL4. Chart
946 show mean ± 95% CI; n shown in chart. Kruskal-Wallis nonparametric test with Dunn's
947 post-hoc test correction for multiple comparisons; **** $P < 0.0001$.
948

949 **Figure 4. ntc regulates basal mitophagy in a parkin and Pink1 independent**
950 **manner.**
951 (**A**, **B**) Confocal microscopy analysis of the *mito-QC* reporter in larval CNS of control
952 and *parkin* mutant alone or with transgenic expression of *ntc* with the pan-neuronal
953 driver *nSyb*-GAL4. Mitolysosomes are evident as GFP-negative/mCherry-positive
954 (red-only) puncta. n shown in chart. One-way ANOVA with Bonferroni post-hoc test
955 correction; * $P < 0.05$, ** $P < 0.01$. Scale bars = 10 μm. (**C**, **D**) Confocal microscopy
956 analysis of the *mito-QC* reporter in larval CNS of control and *Pink1* mutant alone or
957 with transgenic expression of *ntc* with the pan-neuronal driver *nSyb*-GAL4.
958 Mitolysosomes are evident as GFP-negative/mCherry-positive (red-only) puncta. n
959 shown in chart. One-way ANOVA with Bonferroni post-hoc test correction; * $P < 0.05$,
960 ** $P < 0.01$. Scale bar = 10 μm.
961
962 **Figure 5. ntc is required for USP30 knockdown induced basal mitophagy in the**
963 **absence of parkin or Pink1**
964 (**A**, **B**) Confocal microscopy analysis of the mito-QC reporter in larval CNS of control,
965 knockdown of USP30 with the pan-neuronal driver *nSyb*-GAL4 alone or in combination
966 with *ntc* mutants in a *parkin* mutant background. Mitolysosomes are evident as GFP-
967 negative/mCherry-positive (red-only) puncta. n shown in chart. One-way ANOVA with
968 Bonferroni post-hoc test correction; * $P < 0.05$, ** $P < 0.01$, *** $P < 0.001$. Scale bars
969 = 10 μm. (**C**, **D**) Confocal microscopy analysis of the *mito-QC* reporter in larval CNS
970 of control, knockdown of USP30 with the pan-neuronal driver *nSyb*-GAL4 alone or in
971 combination with *ntc* mutants in a *Pink1* mutant background. Mitolysosomes are
972 evident as GFP-negative/mCherry-positive (red-only) puncta. n shown in chart. One-
973 way ANOVA with Bonferroni post-hoc test correction; * $P < 0.05$, ** $P < 0.01$. Scale bar
974 = 10 μm.
975
976 **Figure 6. Manipulating mitophagy by altering levels of USP30 or ntc do not have**
977 **an effect on general autophagy.**
978 (**A**, **B**) Representative immunoblot from whole fly lysates of Atg8a (non-lipidated) I and
979 II (lipidated) in control, USP30 knockdown, ntc overexpression and *ntc* mutant with the
980 ubiquitous driver *da*-GAL4. Data represented as mean ± SD; n shown in chart. One-
981 way ANOVA with Bonferroni post-hoc test correction. (**C**, **D**) Representative
982 immunoblot from whole fly lysates of ref(2)P/p62 in control, USP30 knockdown, ntc
983 overexpression and *ntc* mutant with the ubiquitous driver *da*-GAL4. Data represented
984 as mean ± SD; n shown in chart. One-way ANOVA with Bonferroni post-hoc test
985 correction. (**E**, **F**) Confocal microscopy analysis and quantification of the red-only

986 (autolysosomes) puncta per cell of larval CNS expressing the autophagy flux marker
987 GFP-mCherry-Atg8a in combination with USP30 knockdown, ntc overexpression and
988 *ntc* mutant with the pan-neuronal driver *nSyb*-GAL4. Data represented as mean ±
989 SEM; n shown in chart. One-way ANOVA with Bonferroni post-hoc test correction;
990 Scale bar = 10 μm.
991
992 **Figure 7. Both ntc overexpression and USP30 depletion promote accumulation**
993 **of ubiquitin in the mitochondria and are necessary for pS65-Ub formation.**
994 (**A**) Representative immunoblot and quantification of (**B**) mitochondrial ubiquitin
995 (P4D1) in control, ntc overexpression and USP30 knockdown with the ubiquitous driver
996 *da*-GAL4. Data represented as mean ± SD; n shown in chart. One-way ANOVA with
997 Bonferroni post-hoc test correction; * $P < 0.05$. (**C**, **D**) Representative immunoblot and
998 quantification of mitochondrial pS65-Ub in *parkin* mutants, *ntc* mutants and the double
999 *parkin*:*ntc* mutant. Data represented as mean ± SD; n shown in chart. One-way
1000 ANOVA with Bonferroni post-hoc test correction; * $P < 0.05$, **** $P < 0.0001$. (**E**, **F**)
1001 Representative immunoblot and quantification of mitochondrial pS65-Ub in control and
1002 *parkin* mutants alone or with the transgenic expression of ntc with the ubiquitous driver
1003 *da*-GAL4. Data represented as mean ± SD; n shown in chart. One-way ANOVA with
1004 Bonferroni post-hoc test correction; **** $P < 0.0001$.
1005
1006 **Figure 8. Proposed model for basal and stress-induced mitophagy regulated by**
1007 **ntc, USP30 and parkin.**
1008 In basal, healthy conditions, FBXO7/ntc acts to prime OMM proteins with ubiquitin
1009 counteracted by USP30. This provides a key surveillance checkpoint in quality control
1010 of mitochondrial protein import and/or protein damage. Occasional defects in import or
1011 protein misfolding may lead to a Ub threshold that provokes basal mitophagy.
1012 However, when the need arises in the presence of a stress, for instance, where the
1013 membrane may become depolarised, this population of latent Ub could subsequently
1014 be phosphorylated by Pink1 and amplified by parkin to trigger selective degradation
1015 upon specific stimulation. Created with BioRender.com.
1016
1017
1018 **Figure S1. *mito-QC* reporter targeted to the mitochondrial matrix (*mtx-QC*)**
1019 **reproduces the results observed with the *mito-QC*.**
1020 (**A**, **B**) Confocal microscopy analysis of the *mtx-QC* reporter in larval CNS of control,
1021 *ntc* mutant, *ntc* overexpression and USP30 knockdown with the pan-neuronal driver
1022 *nSyb*-GAL4. Mitolysosomes are evident as GFP-negative/mCherry-positive (red-only)

1023 puncta. n shown in chart. One-way ANOVA with Bonferroni post-hoc test correction; *
1024 $P < 0.05$. Scale bars = 10 μm.
1025
1026 **Figure S2. FBXO7 affects basal mitophagy *in vivo Drosophila* neurons and in a**
1027 **human cell line.**
1028 (**A**, **B**) Confocal microscopy analysis of the *mito-QC* reporter in larval CNS of control
1029 and the transgenic expression of *FBXO7* with the pan-neuronal driver *nSyb*-GAL4.
1030 Mitolysosomes are evident as GFP-negative/mCherry-positive (red-only) puncta; n
1031 shown in chart. One-way ANOVA with Bonferroni post-hoc test correction; *** $P <$
1032 0.001. Scale bar = 10 μm. (**C**) Immunoblot analysis of the knockdown of FBXO7 in
1033 human ARPE-19 cells expressing the *mito-QC* reporter. Arrow shows FBXO7 band; *
1034 shows non-specific band. (**D**, **E**) Confocal microscopy analysis of the *mito-QC* reporter
1035 in ARPE-19 human cell line of control siRNA and FBXO7 siRNA. Mitolysosomes are
1036 evident as GFP-negative/mCherry-positive (red-only) puncta. n shown in chart. Two-
1037 tailed *t* test; ** $P < 0.01$. Scale bars = 10 μm.
1038
1039 **Figure S3. USP30 but neither March5 nor MUL1 can modulate mitophagy *in vivo*.**
1040 (**A**, **B**) Confocal microscopy analysis of the *mito-QC* reporter in 2-day-old adult
1041 thoraces of control and USP30 knockdown with the muscular driver *Mef2*-GAL4.
1042 Mitolysosomes are evident as GFP-negative/mCherry-positive (red-only) puncta. n
1043 shown in chart. Two-tailed *t* test; * $P < 0.05$. Scale bar = 10 μm. (**C**) Climbing ability
1044 of 2-day-old flies expressing *USP30* RNAi with the ubiquitous driver *da*-GAL4 or with
1045 the pan-neuronal driver *nSyb*-GAL4. Chart show mean ± 95% CI and n values.
1046 Kruskal-Wallis nonparametric test with Dunn's post-hoc test correction for multiple
1047 comparisons. (**D**) Climbing ability of 10-day-old flies overexpressing USP30 alone or
1048 in combination with parkin, March5 or Mul1 with the ubiquitous driver *Act*-GAL4. Chart
1049 show mean ± 95% CI and n values. Kruskal-Wallis nonparametric test with Dunn's
1050 post-hoc test correction for multiple comparisons; **** $P < 0.0001$. (**E**, **F**) Confocal
1051 microscopy analysis of the *mito-QC* reporter in larval CNS of control and parkin
1052 overexpression with the pan-neuronal driver *nSyb*-GAL4. Mitolysosomes are evident
1053 as GFP-negative/mCherry-positive (red-only) puncta; n shown in chart. Two-
1054 tailed *t* test. Scale bar = 10 μm. (**G**, **H**) Confocal microscopy analysis of the *mito-QC*
1055 reporter in larval CNS of control and *Mul1* mutant. Mitolysosomes are evident as GFP-
1056 negative/mCherry-positive (red-only) puncta. n shown in chart. Two-tailed *t* test. Scale
1057 bar = 10 μm (**I**, **J**) Confocal microscopy analysis of the *mito-QC* reporter in larval CNS
1058 of control and March5 knockdowns with the pan-neuronal driver *nSyb*-GAL4.

1059 Mitolysosomes are evident as GFP-negative/mCherry-positive (red-only) puncta. n
1060 shown in chart. Two-tailed *t* test. Scale bar = 10 μm.
1061
1062 **Figure S4. Increase in mitophagy levels requires the critical autophagy factor**
1063 **Atg8.**
1064 (**A**, **B**) Confocal microscopy analysis of the *mito-QC* reporter in larval CNS of control,
1065 knockdown of USP30, overexpression of ntc and *ntc* mutant in the *Atg8a* mutant
1066 background with the pan-neuronal driver *nSyb*-GAL4. Mitolysosomes are evident as
1067 GFP-negative/mCherry-positive (red-only) puncta. n shown in chart. One-way ANOVA
1068 with Bonferroni post-hoc test correction; * $P < 0.05$, *** $P < 0.001$. Scale bar = 10 μm.
1069 (**C**, **D**) Confocal microscopy analysis of the *mito-QC* reporter in larval CNS of control
1070 and *parkin* mutant alone or with the USP30 knockdown in the presence or absence of
1071 *Atg8a*, with the pan-neuronal driver *nSyb*-GAL4. Mitolysosomes are evident as GFP-
1072 negative/mCherry-positive (red-only) puncta; n shown in chart. One-way ANOVA with
1073 Bonferroni post-hoc test correction; * $P < 0.05$, ** $P < 0.01$, **** $P < 0.0001$. Scale bar
1074 = 10 μm.
1075
1076 **Figure S5. Analysis of total Ub in subcellular fractions and pS65-Ub upon**
1077 **oxidative stress-induction.**
1078 (**A**) Representative immunoblot of the subcellular fractionation of 2-day-old flies with
1079 the transgenic expression of *ntc* or *USP30* RNAi with the ubiquitous driver *da*-GAL4.
1080 Cytosolic- and mitochondria-enriched fractions are label with Actin and ATP5a,
1081 respectively. **(B)** Representative immunoblot of total ubiquitin (FK2) of 2-day-old flies
1082 in control, *ntc* overexpression and *USP30* knockdown with the ubiquitous driver *da*-
1083 GAL4. **(C)** Representative immunoblot of pS65-Ub levels of 2-day-old flies treated with
1084 paraquat (PQ) in control and *ntc* mutants.

Figure 1

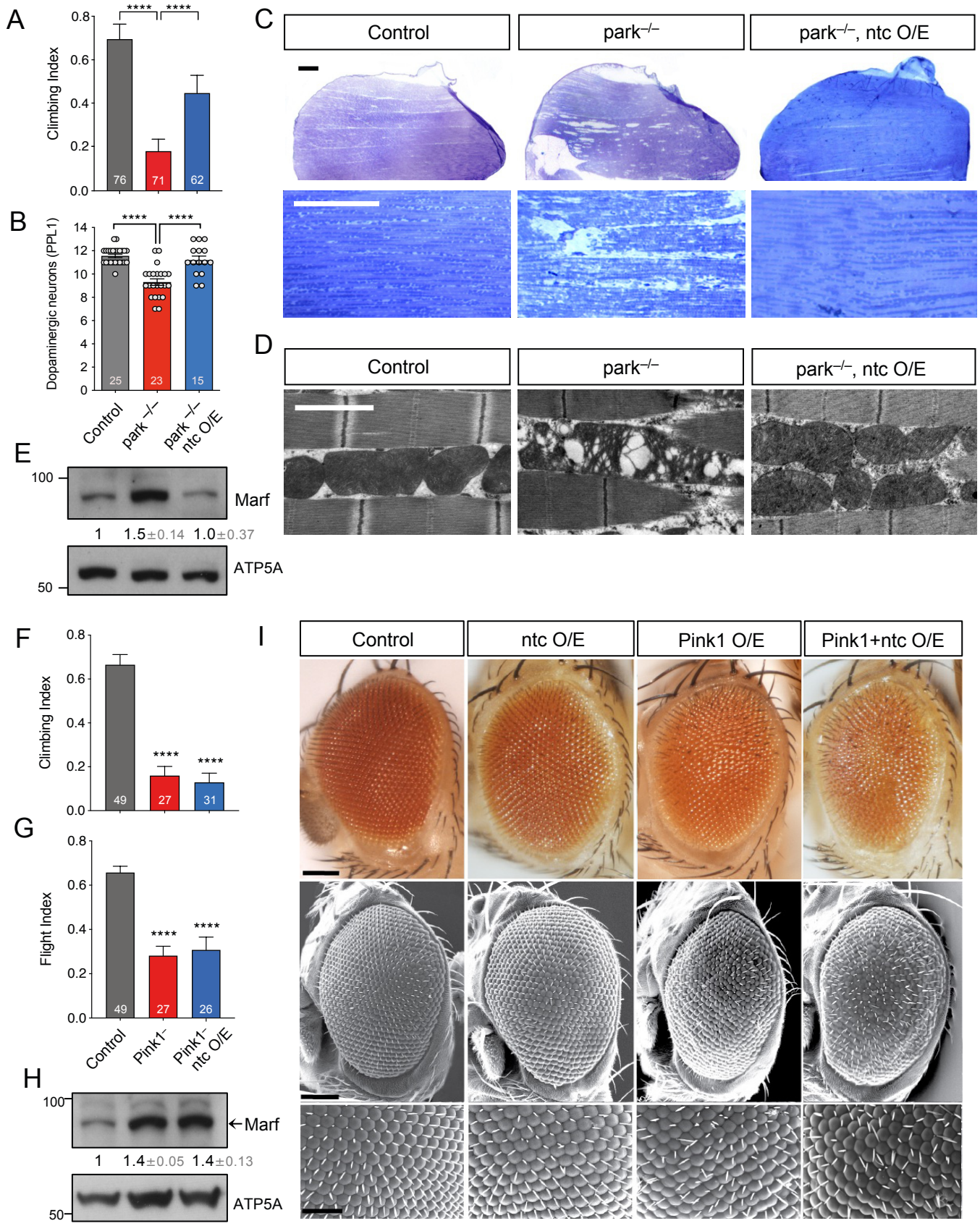
A
Climbing Index
0.8
0.6
0.4
0.2
0.0
****
****
76
71
62
B
Dopaminergic neurons (PPL1)
14
12
10
8
6
4
2
0
****
****
25
23
15
Control
park −/−
park −/− ntc O/E
C
Control
park−/−
park−/−, ntc O/E
D
Control
park−/−
park−/−, ntc O/E
E
100
Marf
1
1.5±0.14
1.0±0.37
50
ATP5A
F
Climbing Index
0.8
0.6
0.4
0.2
0.0
****
****
49
27
31
G
Flight Index
0.8
0.6
0.4
0.2
0.0
****
****
49
27
26
Control
Pink1-
Pink1- ntc O/E
H
100
Marf
1
1.4±0.05
1.4±0.13
50
ATP5A
I
Control
ntc O/E
Pink1 O/E
Pink1+ntc O/E

Figure 2

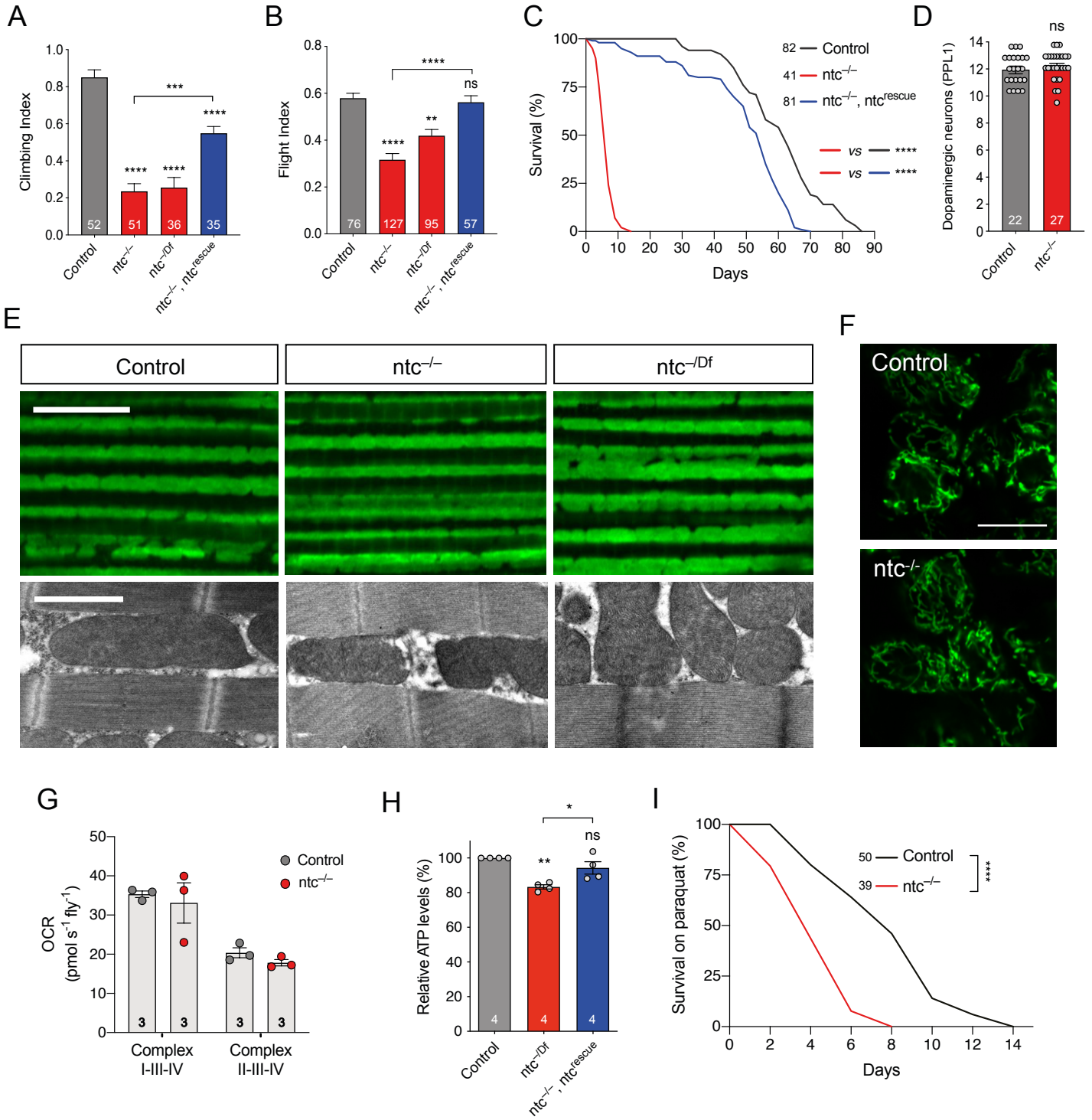
A
Climbing Index
1.0
0.8
0.6
0.4
0.2
0.0
***
****
****
****
52
51
36
35
Control
ntc−/−
ntc−/Df
ntc−/−, ntcrescue
B
Flight Index
0.8
0.6
0.4
0.2
0.0
****
****
**
ns
76
127
95
57
Control
ntc−/−
ntc−/Df
ntc−/−, ntcrescue
C
Survival (%)
100
75
50
25
0
0 10 20 30 40 50 60 70 80 90
Days
82 Control
41 ntc−/−
81 ntc−/−, ntcrescue
vs ****
vs ****
D
Dopaminergic neurons (PPL1)
14
12
10
8
6
4
2
0
ns
22
27
Control
ntc−/−
E
Control
ntc−/−
ntc−/Df
F
Control
ntc-/-
G
OCR
(pmol s-1 fly-1)
50
40
30
20
10
0
Control
ntc−/−
3
3
3
3
Complex
I-III-IV
Complex
II-III-IV
H
Relative ATP levels (%)
100
80
60
40
20
0
*
**
ns
4
4
4
Control
ntc−/Df
ntc−/−, ntcrescue
I
Survival on paraquat (%)
100
75
50
25
0
0 2 4 6 8 10 12 14
Days
50 Control
39 ntc−/−
****

Figure 3

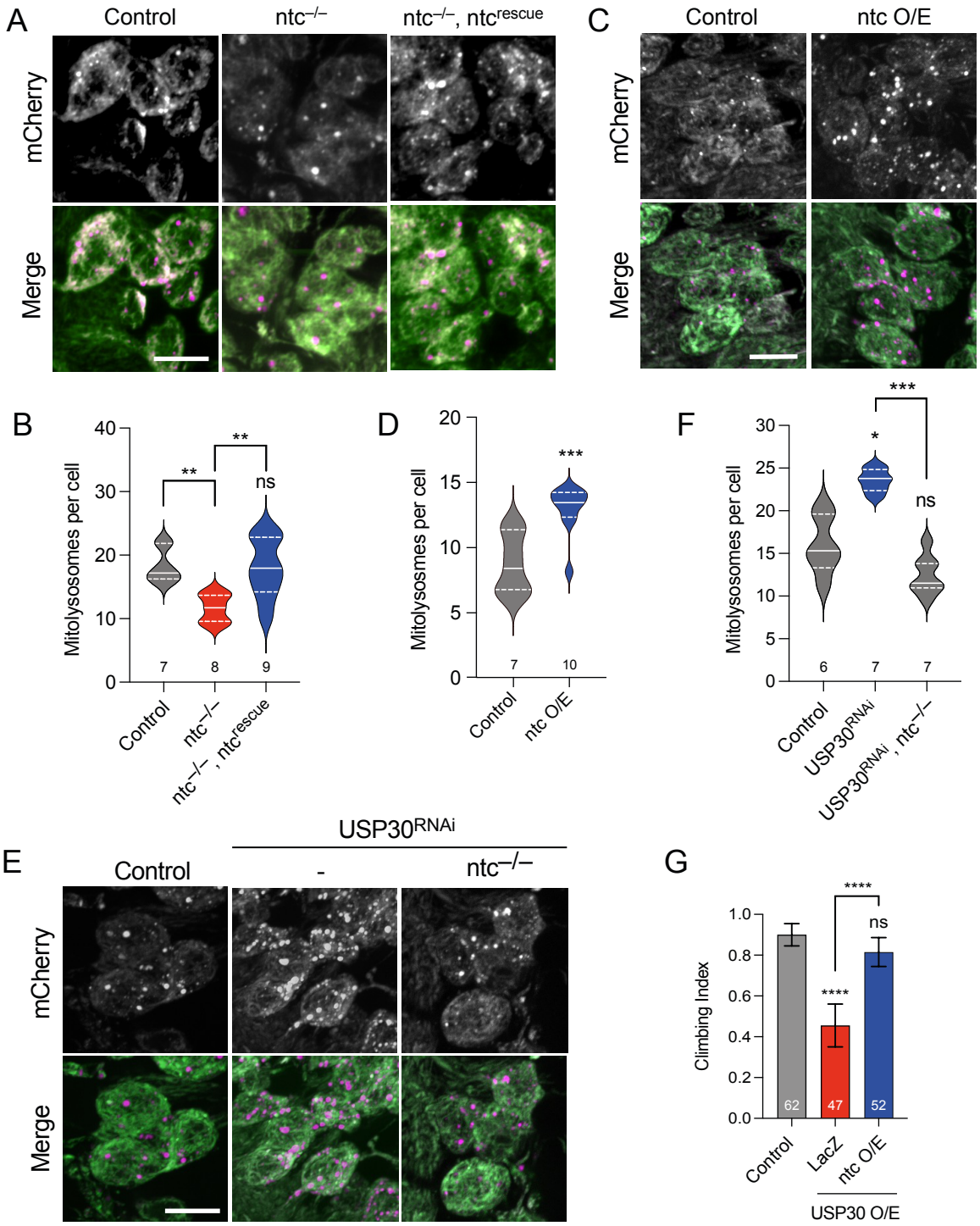
A
Control
ntc−/−
ntc−/−, ntcrescue
mCherry
Merge
C
Control
ntc O/E
mCherry
Merge
B
Mitolysosomes per cell
40
30
20
10
0
**
**
ns
7
8
9
Control
ntc−/−
ntc−/−, ntcrescue
D
Mitolysosmes per cell
20
15
10
5
0
***
7
10
Control
ntc O/E
F
Mitolysosomes per cell
30
25
20
15
10
5
0
*
***
ns
6
7
7
Control
USP30RNAi
USP30RNAi, ntc−/−
E
USP30RNAi
Control
-
ntc−/−
mCherry
Merge
G
Climbing Index
1.0
0.8
0.6
0.4
0.2
0.0
****
****
ns
62
47
52
Control
LacZ
ntc O/E
USP30 O/E

Figure 4

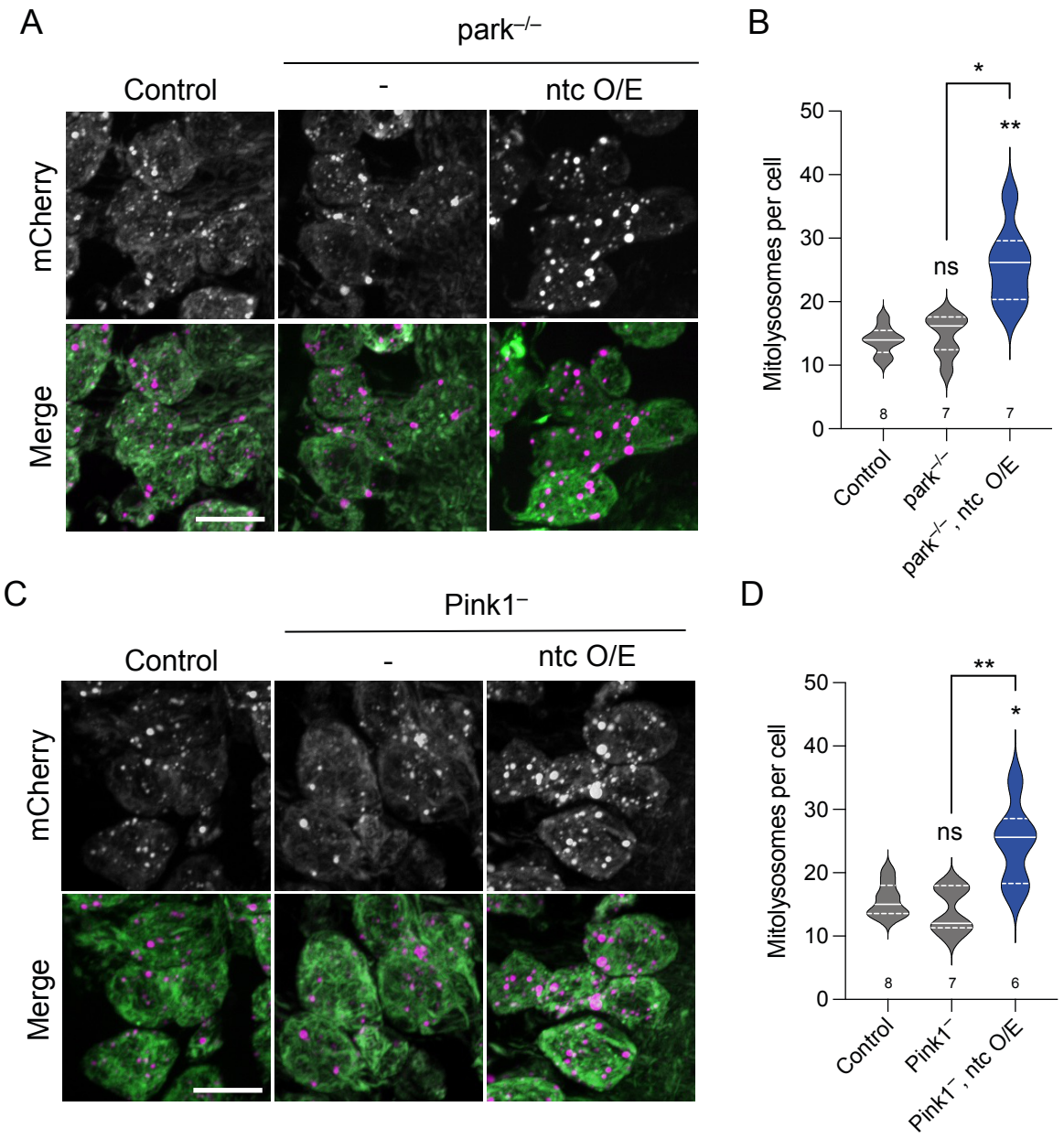
A
park−/−
Control
-
ntc O/E
mCherry
Merge
B
Mitolysosomes per cell
50
40
30
20
10
0
*
**
ns
8
7
7
Control
park−/−
park−/− , ntc O/E
C
Pink1−
Control
-
ntc O/E
mCherry
Merge
D
Mitolysosomes per cell
50
40
30
20
10
0
**
*
ns
8
7
6
Control
Pink1−
Pink1− , ntc O/E

Figure 5

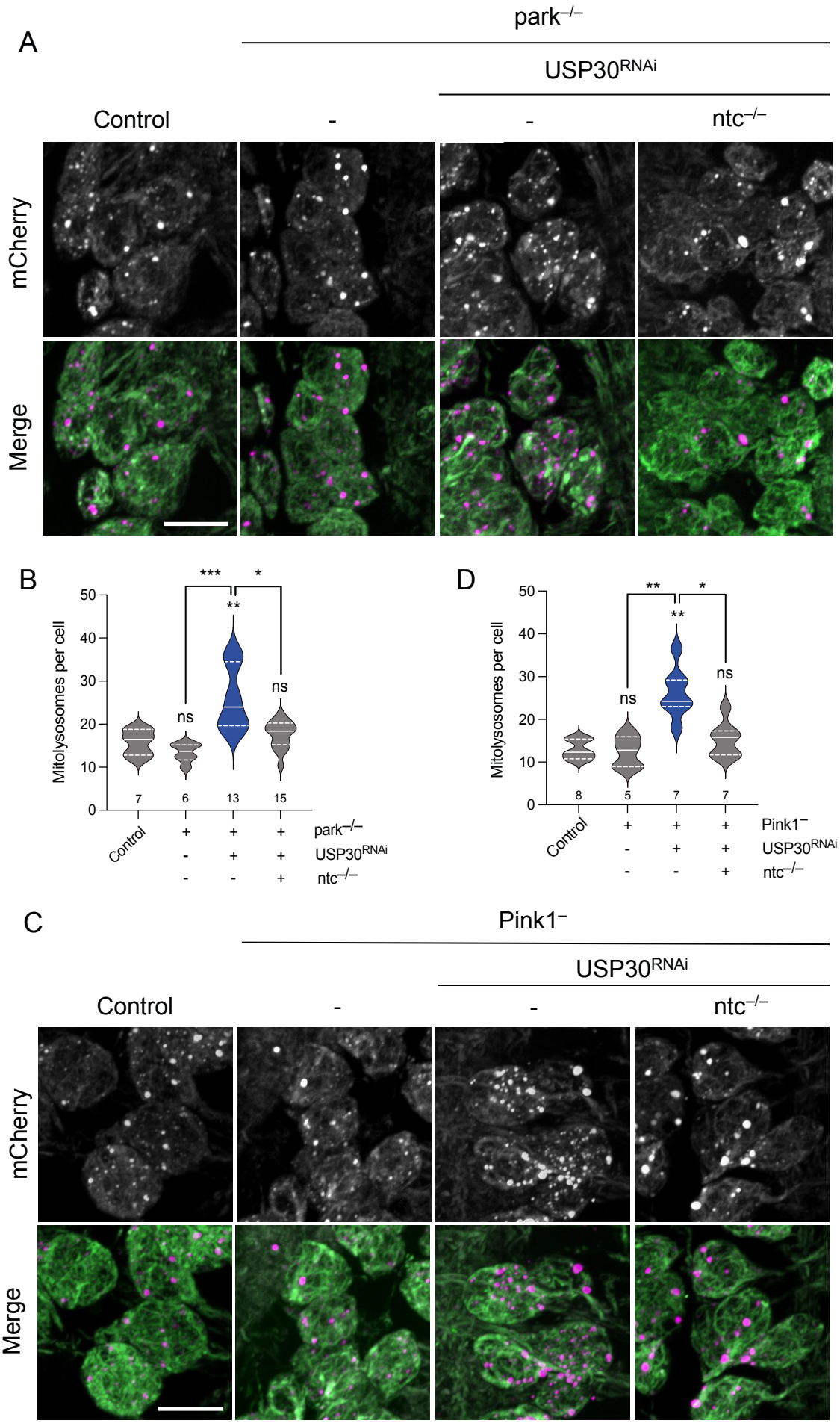
A
park–/–
USP30RNAi
Control
-
-
ntc–/–
mCherry
Merge
B
Mitolysosomes per cell
50
40
30
20
10
0
***
*
**
ns
ns
7
6
13
15
Control
+
+
+
park–/–
-
+
+
USP30RNAi
-
-
+
ntc–/–
D
Mitolysosomes per cell
50
40
30
20
10
0
**
*
**
ns
ns
8
5
7
7
Control
+
+
+
Pink1–
-
+
+
USP30RNAi
-
-
+
ntc–/–
C
Pink1–
USP30RNAi
Control
-
-
ntc–/–
mCherry
Merge

Figure 6

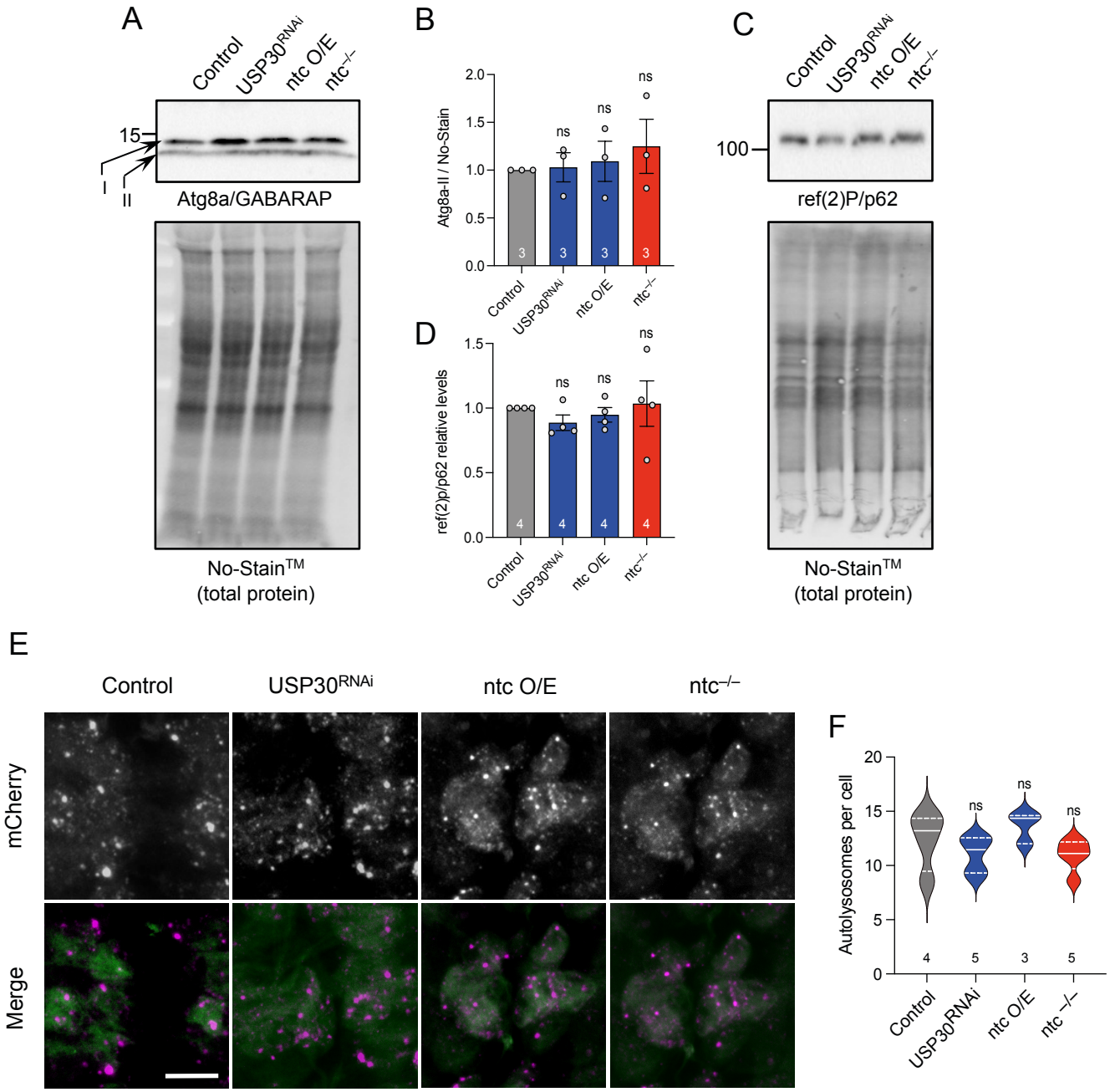
A
Control
USP30RNAi
ntc O/E
ntc−/−
15
I
II
Atg8a/GABARAP
No-Stain™
(total protein)
B
Atg8a-II / No-Stain
2.0
1.5
1.0
0.5
0.0
ns
3
Control
USP30RNAi
ntc O/E
ntc−/−
C
100
ref(2)P/p62
No-Stain™
(total protein)
D
ref(2)p/p62 relative levels
4
E
Control
USP30RNAi
ntc O/E
ntc−/−
mCherry
Merge
F
Autolysosomes per cell
20
15
10
5
0
4
5
3
5

Figure 7

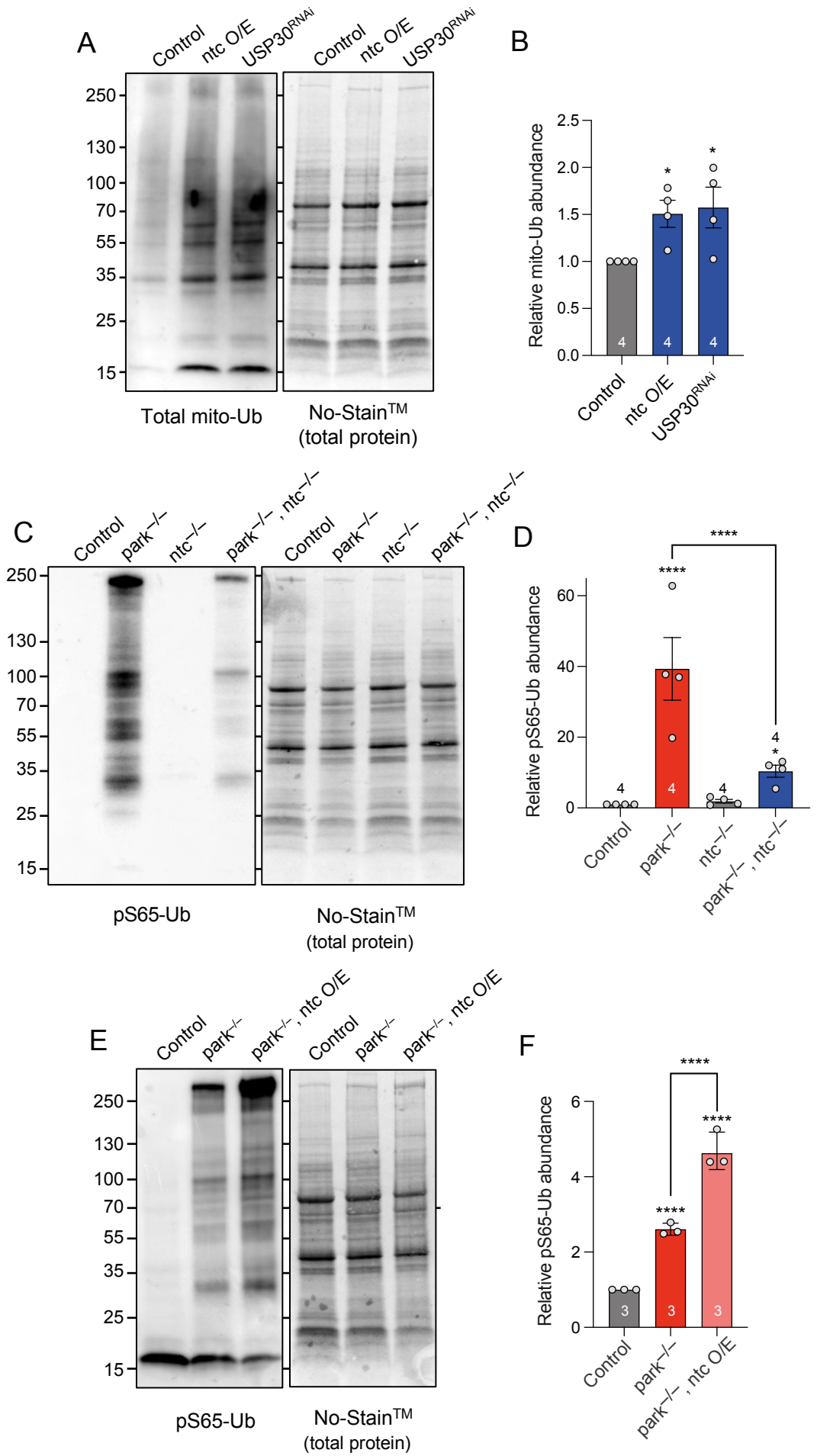
A
Control
ntc O/E
USP30RNAi
Control
ntc O/E
USP30RNAi
250
130
100
70
55
35
25
15
Total mito-Ub
No-Stain™
(total protein)
B
Relative mito-Ub abundance
2.5
2.0
1.5
1.0
0.5
0.0
*
*
4
4
4
Control
ntc O/E
USP30RNAi
C
Control
park−/−
ntc−/−
park−/−, ntc−/−
Control
park−/−
ntc−/−
park−/−, ntc−/−
250
130
100
70
55
35
25
15
pS65-Ub
No-Stain™
(total protein)
D
Relative pS65-Ub abundance
60
40
20
0
****
****
4
4
4
4
*
Control
park−/−
ntc−/−
park−/−, ntc−/−
E
Control
park−/−
park−/−, ntc O/E
Control
park−/−
park−/−, ntc O/E
250
130
100
70
55
35
25
15
pS65-Ub
No-Stain™
(total protein)
F
Relative pS65-Ub abundance
6
4
2
0
****
****
****
3
3
3
Control
park−/−
park−/−, ntc O/E

Figure 8

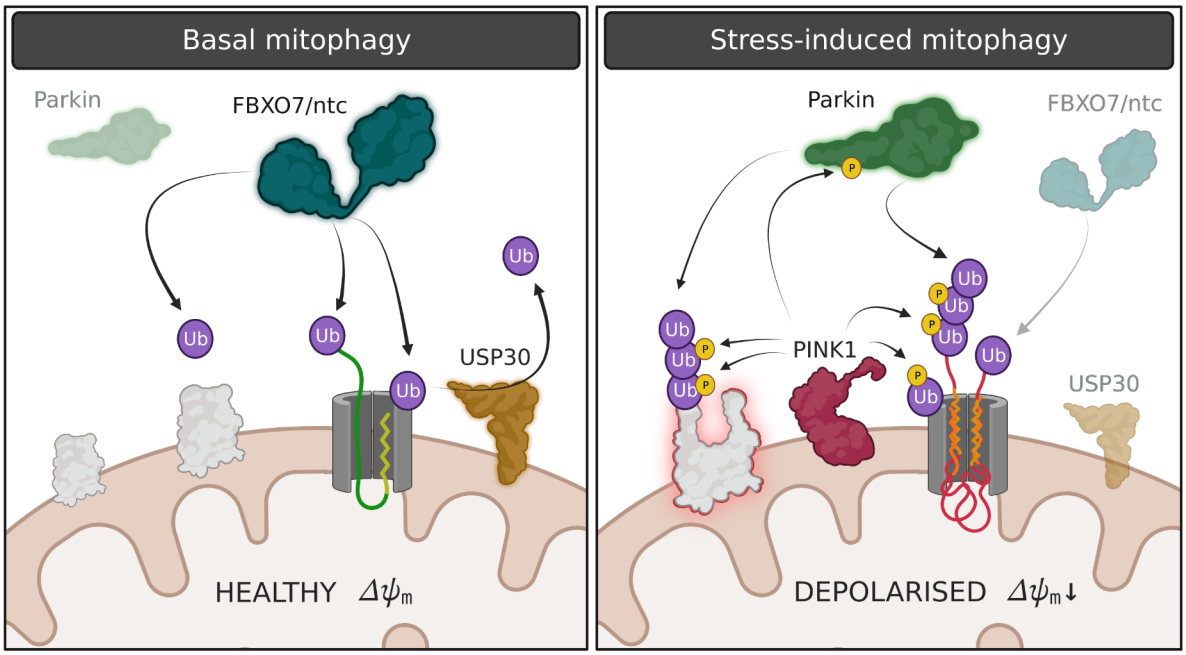
Basal mitophagy
Parkin
FBXO7/ntc
Ub
Ub
Ub
Ub
USP30
HEALTHY $\Delta\psi_m$
Stress-induced mitophagy
Parkin
FBXO7/ntc
P
Ub
Ub
Ub
Ub
Ub
Ub
Ub
Ub
Ub
Ub
PINK1
USP30
DEPOLARISED $\Delta\psi_m\downarrow$

Supplementary Figure 1

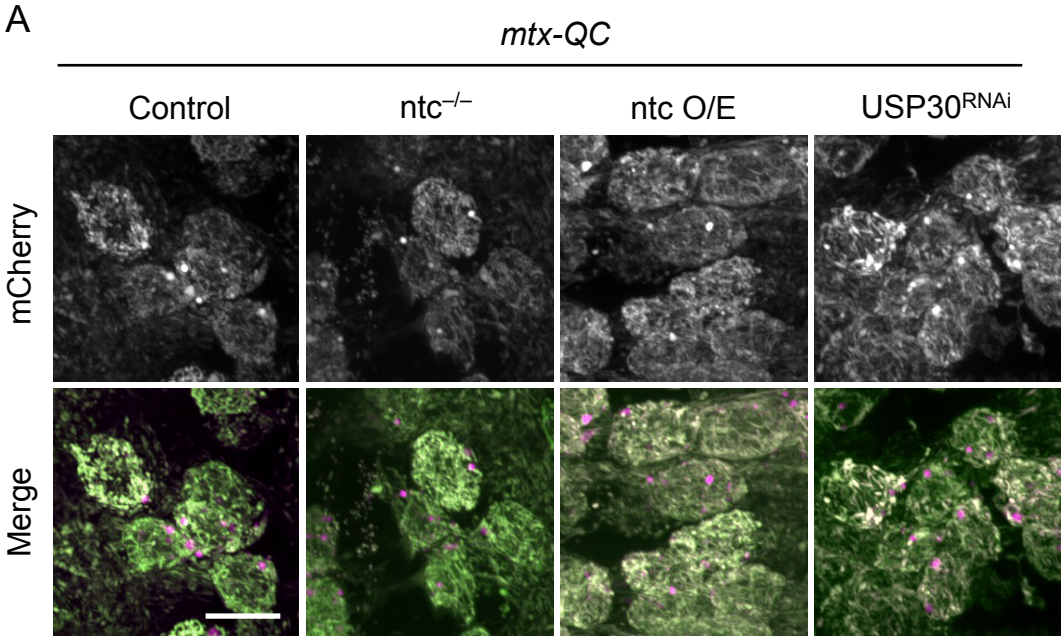

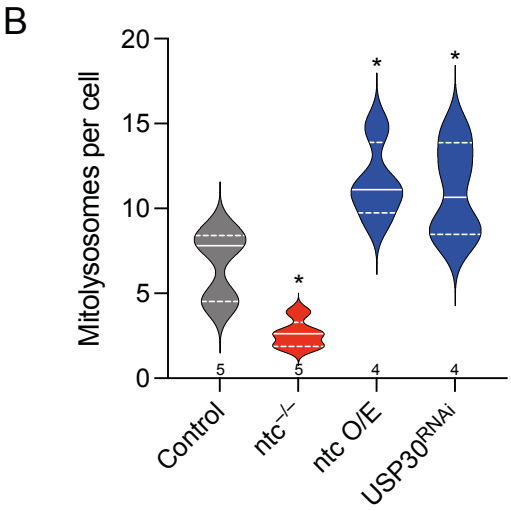

Supplementary Figure 2

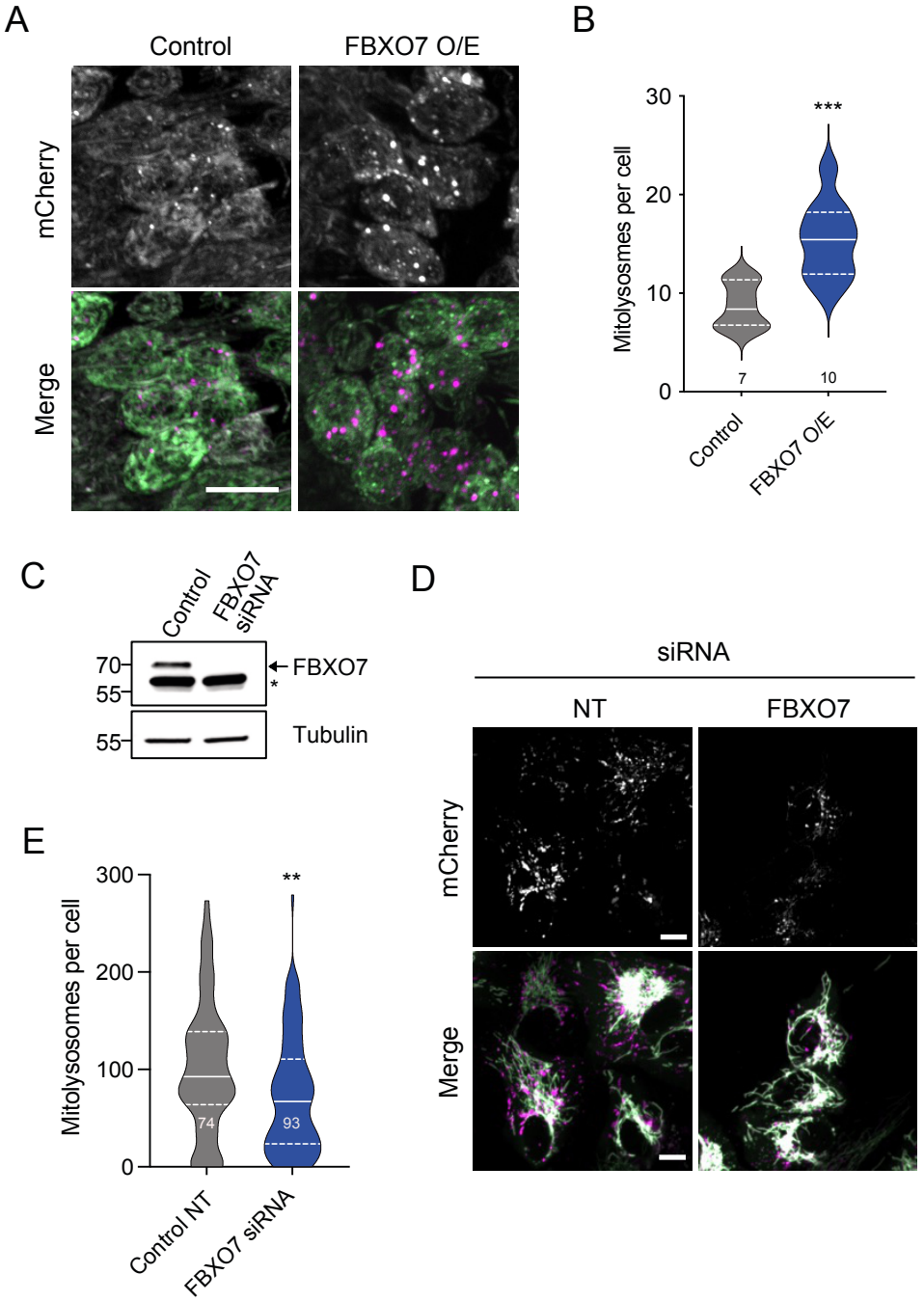

Supplementary Figure 3

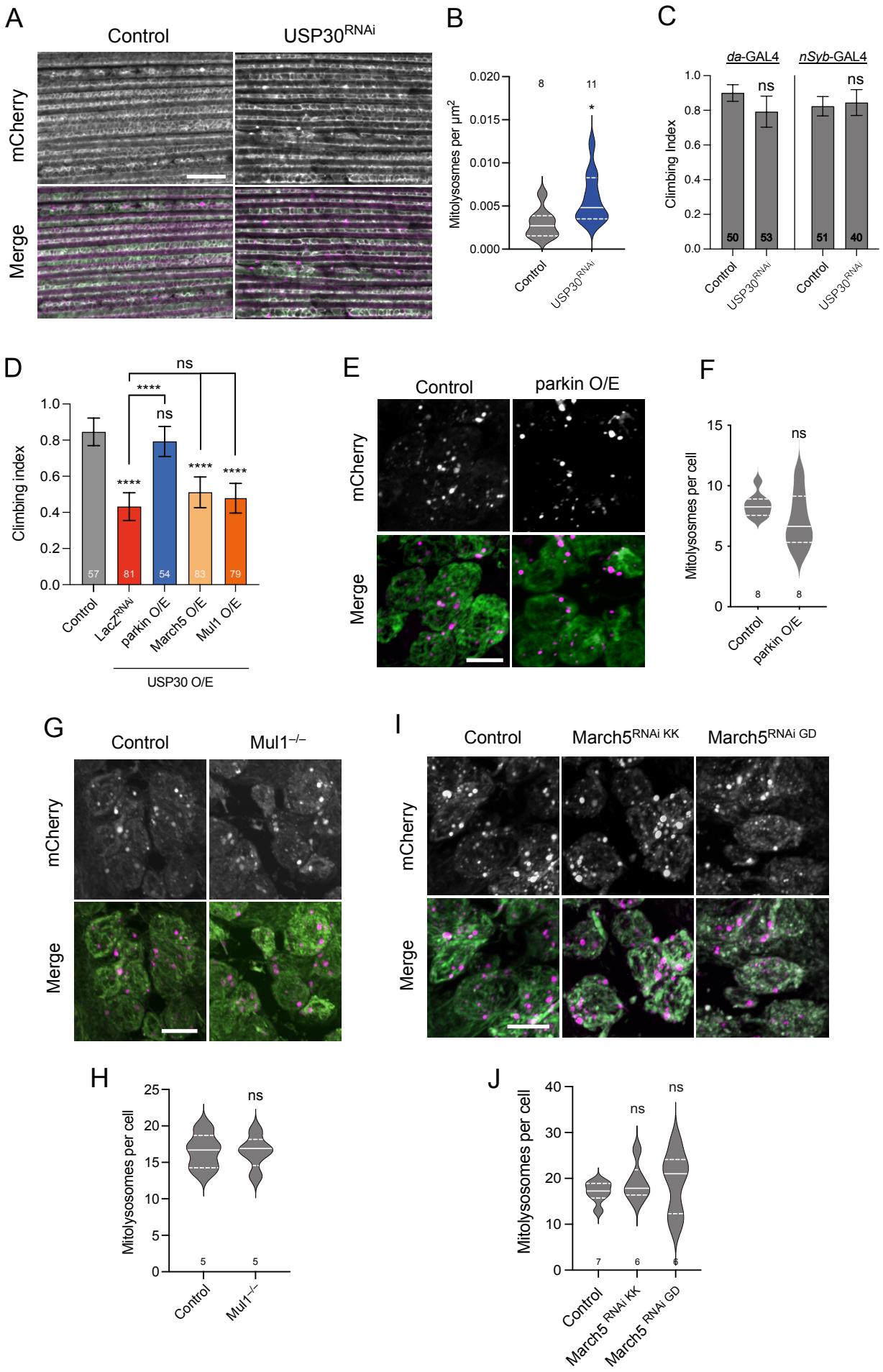

Supplementary Figure 4

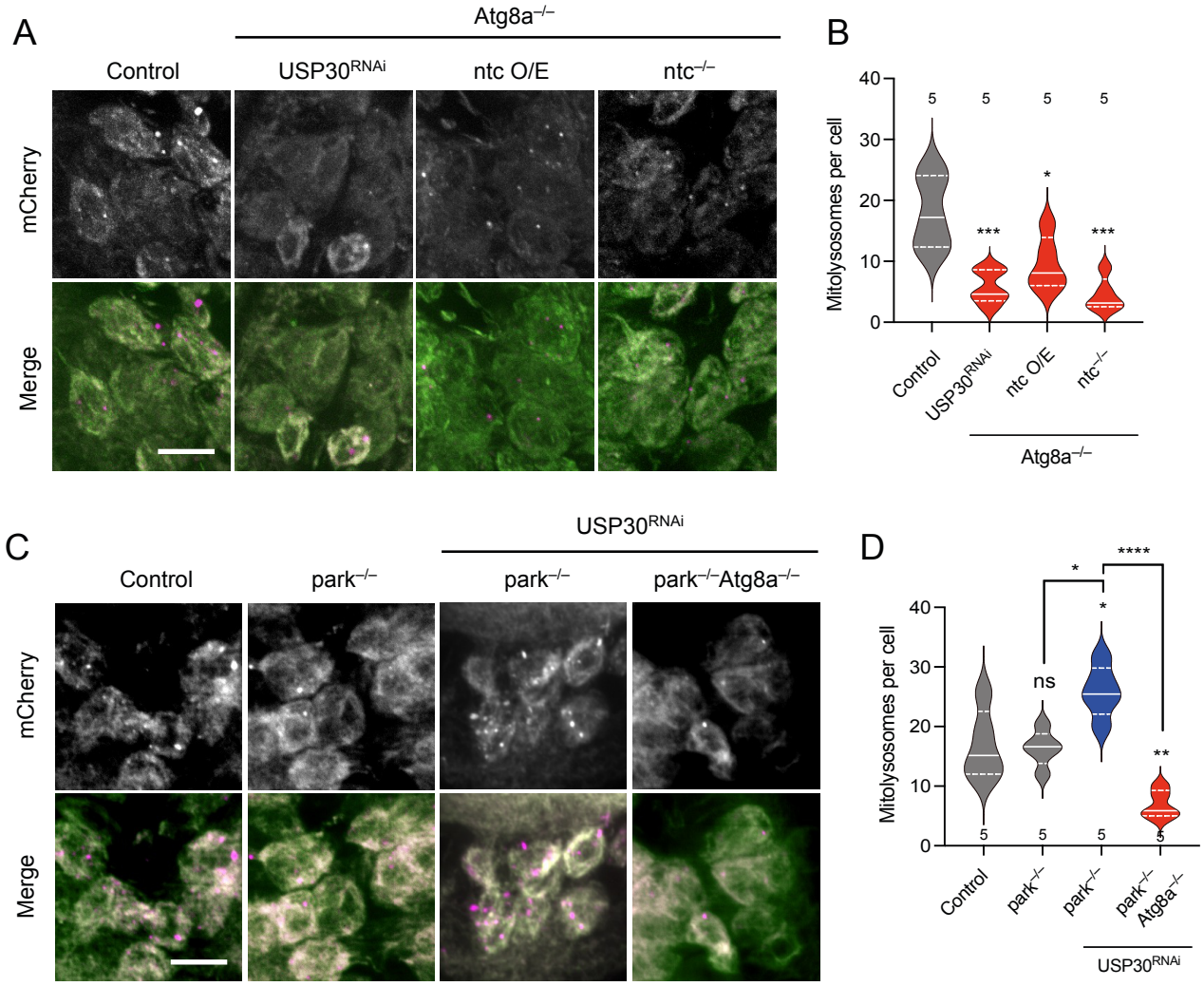

Supplementary Figure 5

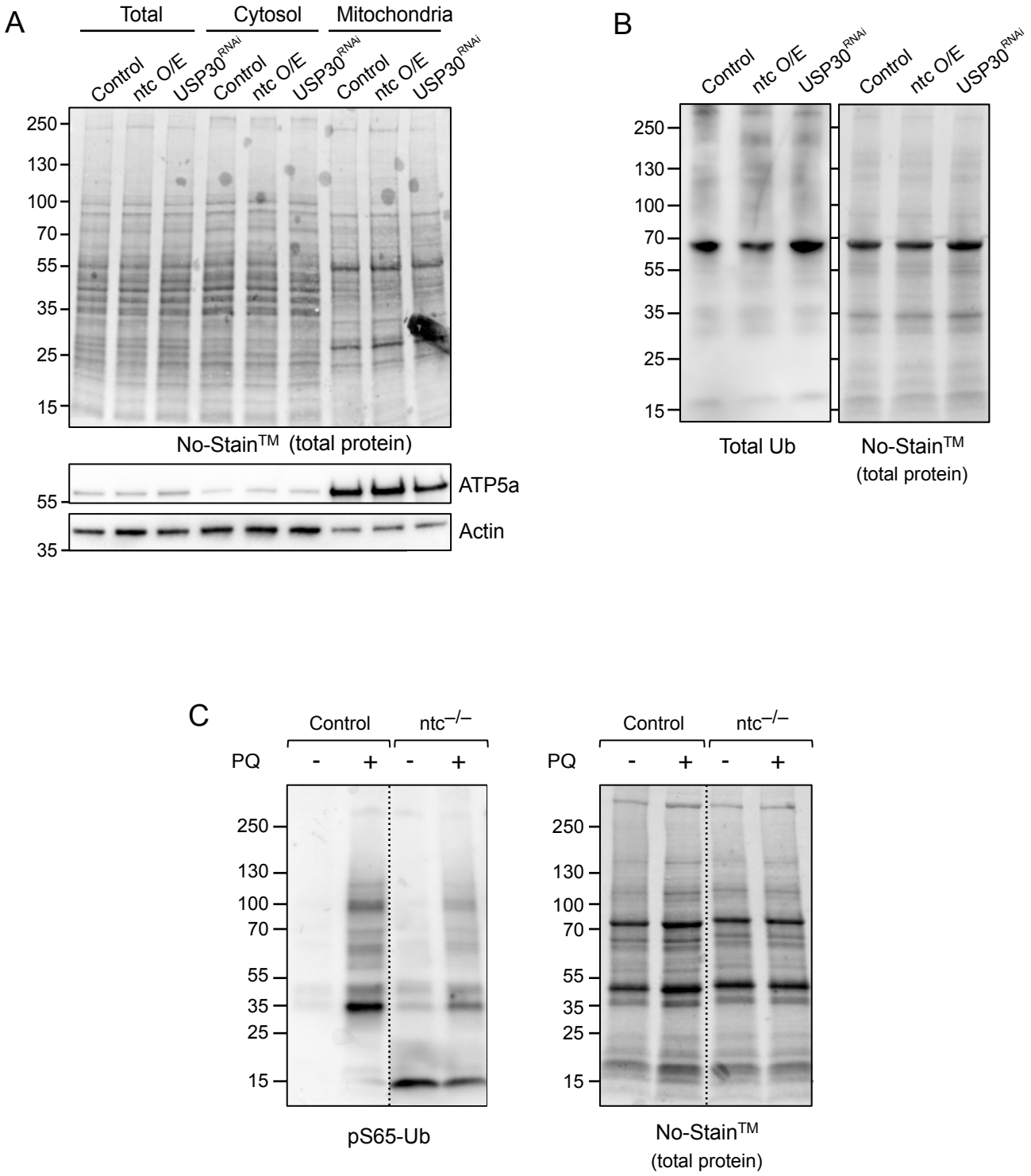

Supplementary Table 1. Details of full genotypes used in this study. More details of each line can be found in Methods.

Figure 1	
Label	**Genotype**
A	
Control	UAS-LacZ/+; da-GAL4/+
park$^{-/-}$	UAS-LacZ/+; da-GAL4, park^{25}/park^{25}
park$^{-/-}$; ntc O/E	UAS-ntc/+; da-GAL4, park^{25}/park^{25}
B	
Control	UAS-LacZ/+; da-GAL4/+
park$^{-/-}$	UAS-LacZ/+; da-GAL4, park^{25}/park^{25}
park$^{-/-}$; ntc O/E	UAS-ntc/+; da-GAL4, park^{25}/park^{25}
C	
Control	UAS-LacZ/+; da-GAL4/+
park$^{-/-}$	UAS-LacZ/+; da-GAL4, park^{25}/park^{25}
park$^{-/-}$; ntc	UAS-ntc/+; da-GAL4, park^{25}/park^{25}
D	
Control	UAS-LacZ/+; da-GAL4/+
park$^{-/-}$	UAS-LacZ/+; da-GAL4, park^{25}/park^{25}
park$^{-/-}$; ntc O/E	UAS-ntc/+; da-GAL4, park^{25}/park^{25}
E	
Control	UAS-LacZ/+; da-GAL4/+
park$^{-/-}$	UAS-LacZ/+; da-GAL4, park^{25}/park^{25}
park$^{-/-}$; ntc O/E	UAS-ntc/+; da-GAL4, park^{25}/park^{25}
F	
Control	UAS-LacZ/+; da-GAL4/+
Pink1^{-}	Pink1^{B9}/Y; UAS-LacZ/+; da-GAL4/+

Pink1^{-}; ntc O/E	Pink1^{B9}/Y; UAS-ntc/+; da-GAL4/+
G	
Control	UAS-LacZ/+; da-GAL4/+
Pink1^{-}	Pink1^{B9}/Y; UAS-LacZ/+; da-GAL4/+
Pink1^{-}; ntc O/E	Pink1^{B9}/Y; UAS-ntc/+; da-GAL4/+
H	
Control	UAS-LacZ/+; da-GAL4/+
Pink1^{-}	Pink1^{B9}/Y; UAS-LacZ/+; da-GAL4/+
Pink1^{-}; ntc O/E	Pink1^{B9}/Y; UAS-ntc/+; da-GAL4/+
I	
Control	GMR-GAL4/UAS-LacZ
ntc O/E	GMR-GAL4, UAS-LacZ/UAS-ntc
Pink1 O/E	GMR-GAL4, UAS-Pink1/UAS-LacZ
Pink1+ntc O/E	GMR-GAL4, UAS-Pink1/UAS-ntc

Figure 2	
Label	**Genotype**
A	
Control	UAS-LacZ/+; da-GAL4/+
ntc$^{-/-}$	ntc^{ms771}/ntc^{ms771}
ntc$^{-/Df}$	ntc^{ms771}/Df(3L)Exel6097
ntc$^{-/-}$, ntc^{rescue}	UAS-ntc; da-GAL4, ntc^{ms771}/ ntc^{ms771}
B	
Control	UAS-LacZ/+; da-GAL4/+
ntc$^{-/-}$	ntc^{ms771}/ntc^{ms771}
ntc$^{-/Df}$	ntc^{ms771}/Df(3L)Exel6097

ntc$^{-/-}$, ntc^{rescue}	UAS-ntc; da-GAL4, ntc^{ms771}/ ntc^{ms771}
C	
Control	w^{1118}
ntc$^{-/-}$	ntc^{ms771}/ntc^{ms771}
ntc$^{-/-}$, ntc^{rescue}	UAS-ntc; da-GAL4, ntc^{ms771}/ntc^{ms771}
D	
Control	w^{1118}
ntc$^{-/-}$	ntc^{ms771}/ntc^{ms771}
E	
Control	UAS-LacZ/+; da-GAL4/+
ntc$^{-/-}$	ntc^{ms771}/ntc^{ms771}
ntc$^{-/Df}$	ntc^{ms771}/Df(3L)Exel6097
F	
Control	w^{1118}
ntc$^{-/-}$	ntc^{ms771}/ntc^{ms771}
G	
Control	w^{1118}
ntc$^{-/-}$	ntc^{ms771}/ntc^{ms771}
H	
Control	w^{1118}
ntc$^{-/-}$	ntc^{ms771}/ntc^{ms771}
ntc$^{-/-}$, ntc^{rescue}	UAS-ntc; da-GAL4, ntc^{ms771}/ntc^{ms771}
I	
Control	w^{1118}
ntc$^{-/-}$	ntc^{ms771}/ntc^{ms771}

Figure 3	
Label	**Genotype**
A	
Control	mito-QC/UAS-LacZ^{RNAi}; nSyb-GAL4/+
ntc$^{-/-}$	mito-QC/UAS-LacZ^{RNAi}; nSyb-GAL4, ntc^{ms771}/ntc^{ms771}
ntc$^{-/-}$, ntc^{rescue}	mito-QC/UAS-ntc; nSyb-GAL4, ntc^{ms771}/ntc^{ms771}
B	
Control	mito-QC/UAS-LacZ^{RNAi}; nSyb-GAL4/+
ntc$^{-/-}$	mito-QC/UAS-LacZ^{RNAi}; nSyb-GAL4, ntc^{ms771}/ntc^{ms771}
ntc$^{-/-}$, ntc^{rescue}	mito-QC/UAS-ntc; nSyb-GAL4, ntc^{ms771}/ntc^{ms771}
C	
Control	mito-QC/UAS-LacZ^{RNAi}; nSyb-GAL4/+
ntc O/E	mito-QC/UAS-ntc; nSyb-GAL4/+
D	
Control	mito-QC/UAS-LacZ^{RNAi}; nSyb-GAL4/+
ntc O/E	mito-QC/UAS-ntc; nSyb-GAL4/+
E	
Control	mito-QC/UAS-LacZ^{RNAi}; nSyb-GAL4/+
USP30^{RNAi}	mito-QC/UAS-USP30^{RNAi}; nSyb-GAL4/+
USP30^{RNAi}, ntc$^{-/-}$	mito-QC/UAS-USP30^{RNAi}; nSyb-GAL4, ntc^{ms771}/ntc^{ms771}
F	
Control	mito-QC/UAS-LacZ^{RNAi}; nSyb-GAL4/+
USP30^{RNAi}	mito-QC/UAS-USP30^{RNAi}; nSyb-GAL4/+
USP30^{RNAi}, ntc$^{-/-}$	mito-QC/UAS-USP30^{RNAi}; nSyb-GAL4, ntc^{ms771}/ntc^{ms771}
G	
Control	Act-GAL4/UAS-LacZ

USP30 O/E + LacZ	Act-GAL4, UAS-USP30/UAS-LacZ
USP30 O/E + ntc O/E	Act-GAL4, UAS-USP30/UAS-ntc

Figure 4	
Label	**Genotype**
A	
Control	mito-QC/UAS-LacZ^{RNAi}; nSyb-GAL4/+
park$^{-/-}$	mito-QC/UAS-LacZ^{RNAi}; nSyb-GAL4, park^{25}/park^{25}
park$^{-/-}$, ntc O/E	mito-QC/UAS-ntc; nSyb-GAL4, park^{25}/park^{25}
B	
Control	mito-QC/UAS-LacZ^{RNAi}; nSyb-GAL4/+
park$^{-/-}$	mito-QC/UAS-LacZ^{RNAi}; nSyb-GAL4, park^{25}/park^{25}
park$^{-/-}$, ntc O/E	mito-QC/UAS-ntc; nSyb-GAL4, park^{25}/park^{25}
C	
Control	mito-QC/UAS-LacZ^{RNAi}; nSyb-GAL4/+
Pink1^{-}	Pink1^{B9}/Y; mito-QC/UAS-LacZ^{RNAi}; nSyb-GAL4/+
Pink1^{-}, ntc O/E	Pink1^{B9}/Y; mito-QC/UAS-ntc; nSyb-GAL4/+
D	
Control	mito-QC/UAS-LacZ^{RNAi}; nSyb-GAL4/+
Pink1^{-}	Pink1^{B9}/Y; mito-QC/UAS-LacZ^{RNAi}; nSyb-GAL4/+
Pink1^{-}, ntc O/E	Pink1^{B9}/Y; mito-QC/UAS-ntc; nSyb-GAL4/+

Figure 5	
Label	**Genotype**
A	
Control	mito-QC/UAS-LacZ^{RNAi}; nSyb-GAL4/+

park$^{-/-}$	mito-QC/UAS-LacZ^{RNAi}; nSyb-GAL4, park^{25}/park^{25}
park$^{-/-}$, USP30^{RNAi}	mito-QC/UAS-USP30^{RNAi}; nSyb-GAL4, park^{25}/park^{25}
park$^{-/-}$, USP30^{RNAi}, ntc$^{-/-}$	mito-QC/UAS-USP30^{RNAi}; nSyb-GAL4, park^{25}, PBac{WH}CG10855^{f07259}/ntc^{ms771}
B	
Control	mito-QC/UAS-LacZ^{RNAi}; nSyb-GAL4/+
park$^{-/-}$	mito-QC/UAS-LacZ^{RNAi}; nSyb-GAL4, park^{25}/park^{25}
park$^{-/-}$, USP30^{RNAi}	mito-QC/UAS-USP30^{RNAi}; nSyb-GAL4, park^{25}/park^{25}
park$^{-/-}$, USP30^{RNAi}, ntc$^{-/-}$	mito-QC/UAS-USP30^{RNAi}; nSyb-GAL4, park^{25}, PBac{WH}CG10855^{f07259}/ntc^{ms771}
C	
Control	mito-QC/ UAS-LacZ^{RNAi}; nSyb-GAL4/+
Pink1^{-}	Pink1^{B9}/Y; mito-QC/UAS-LacZ^{RNAi}; nSyb-GAL4/+
Pink1^{-}, USP30^{RNAi}	Pink1^{B9}/Y; mito-QC/UAS-USP30^{RNAi}; nSyb-GAL4/+
Pink1^{-}, USP30^{RNAi}, ntc$^{-/-}$	Pink1^{B9}/Y; mito-QC/UAS-USP30^{RNAi}; nSyb-GAL4, ntc^{ms771}/ntc^{ms771}
D	
Control	mito-QC/ UAS-LacZ^{RNAi}; nSyb-GAL4/+
Pink1^{-}	Pink1^{B9}/Y; mito-QC/UAS-LacZ^{RNAi}; nSyb-GAL4/+
Pink1^{-}, USP30^{RNAi}	Pink1^{B9}/Y; mito-QC/UAS-USP30^{RNAi}; nSyb-GAL4/+
Pink1^{-}, USP30^{RNAi}, ntc$^{-/-}$	Pink1^{B9}/Y; mito-QC/UAS-USP30^{RNAi}; nSyb-GAL4, ntc^{ms771}/ntc^{ms771}

Figure 6	
Label	**Genotype**
A	
Control	UAS-LacZ/+; da-GAL4/+
USP30^{RNAi}	UAS-USP30^{RNAi}/+; da-GAL4/+

ntc O/E	UAS-ntc/+; da-GAL4/+
ntc$^{-/-}$	ntc^{ms771}/ntc^{ms771}
B	
Control	UAS-LacZ/+; da-GAL4/+
USP30^{RNAi}	UAS-USP30^{RNAi}/+; da-GAL4/+
ntc O/E	UAS-ntc/+; da-GAL4/+
ntc$^{-/-}$	ntc^{ms771}/ntc^{ms771}
C	
Control	UAS-LacZ/+; da-GAL4/+
USP30^{RNAi}	UAS-USP30^{RNAi}/+; da-GAL4/+
ntc O/E	UAS-ntc/+; da-GAL4/+
ntc$^{-/-}$	ntc^{ms771}/ntc^{ms771}
D	
Control	UAS-LacZ/+; da-GAL4/+
USP30^{RNAi}	UAS-USP30^{RNAi}/+; da-GAL4/+
ntc O/E	UAS-ntc/+; da-GAL4/+
ntc$^{-/-}$	ntc^{ms771}/ntc^{ms771}
E	
Control	UAS-GFP-mCherry-Atg8a/UAS-LacZ^{RNAi}/+; nSyb-GAL4/+
USP30^{RNAi}	UAS-GFP-mCherry-Atg8a/UAS-USP30^{RNAi}/+; nSyb-GAL4/+
ntc O/E	UAS-GFP-mCherry-Atg8a/UAS-ntc/+; nSyb-GAL4/+
ntc$^{-/-}$	UAS-GFP-mCherry-Atg8a/UAS-LacZ^{RNAi}/+; nSyb-GAL4, ntc^{ms771}/ntc^{ms771}
F	
Control	UAS-GFP-mCherry-Atg8a/UAS-LacZ^{RNAi}/+; nSyb-GAL4/+
USP30^{RNAi}	UAS-GFP-mCherry-Atg8a/UAS-USP30^{RNAi}/+; nSyb-GAL4/+

ntc O/E	UAS-GFP-mCherry-Atg8a/UAS-ntc/+; nSyb-GAL4/+
ntc$^{-/-}$	UAS-GFP-mCherry-Atg8a/UAS-LacZ^{RNAi}/+; nSyb-GAL4, ntc^{ms771}/ntc^{ms771}

Figure 7	
Label	**Genotype**
A	
Control	UAS-LacZ/+; da-GAL4/+
ntc O/E	UAS-ntc/+; da-GAL4/+
USP30^{RNAi}	UAS-USP30^{RNAi}/+; da-GAL4/+
B	
Control	UAS-LacZ/+; da-GAL4/+
ntc O/E	UAS-ntc/+; da-GAL4/+
USP30^{RNAi}	UAS-USP30^{RNAi}/+; da-GAL4/+
C	
Control	w^{1118}
park$^{-/-}$	park^{25}/park^{25}
ntc$^{-/-}$	ntc^{ms771}/PBac{WH}CG10855^{f07259}
park$^{-/-}$, ntc$^{-/-}$	park^{25}, ntc^{ms771}/park^{25}, PBac{WH}CG10855^{f07259}
D	
Control	w^{1118}
park$^{-/-}$	park^{25}/park^{25}
ntc$^{-/-}$	ntc^{ms771}/PBac{WH}CG10855^{f07259}
park$^{-/-}$, ntc$^{-/-}$	park^{25}, ntc^{ms771}/park^{25}, PBac{WH}CG10855^{f07259}
E	
Control	UAS-LacZ/+; da-GAL4/+
park$^{-/-}$	UAS-LacZ/+; da-GAL4, park^{25}/park^{25}

park$^{-/-}$; ntc O/E	UAS-ntc/+; da-GAL4, park^{25}/park^{25}
F	
Control	UAS-LacZ/+; da-GAL4/+
park$^{-/-}$	UAS-LacZ/+; da-GAL4, park^{25}/park^{25}
park$^{-/-}$; ntc O/E	UAS-ntc/+; da-GAL4, park^{25}/park^{25}

Supplementary Figure 1	
Label	**Genotype**
A	
Control	mtx-QC/UAS-LacZ^{RNAi}; nSyb-GAL4/+
USP30^{RNAi}	mtx-QC/UAS-USP30^{RNAi}; nSyb-GAL4/+
ntc	mtx-QC/UAS-ntc; nSyb-GAL4/+
ntc$^{-/-}$	mtx-QC/UAS-LacZ^{RNAi}; nSyb-GAL4, ntc^{ms771}/ntc^{ms771}
B	
Control	mtx-QC/UAS-LacZ^{RNAi}; nSyb-GAL4/+
USP30^{RNAi}	mtx-QC/UAS-USP30^{RNAi}; nSyb-GAL4/+
ntc	mtx-QC/UAS-ntc; nSyb-GAL4/+
ntc$^{-/-}$	mtx-QC/UAS-LacZ^{RNAi}; nSyb-GAL4, ntc^{ms771}/ntc^{ms771}

Supplementary Figure 2	
Label	**Genotype**
A	
Control	mito-QC/UAS-LacZ^{RNAi}; nSyb-GAL4/+
FBXO7 O/E	mito-QC/UAS-FBXO7; nSyb-GAL4/+
B	
Control	mito-QC/UAS-LacZ^{RNAi}; nSyb-GAL4/+

FBXO7 O/E	mito-QC/UAS-FBXO7; nSyb-GAL4/+

Supplementary Figure 3	
Label	**Genotype**
A	
Control	Mef2-GAL4/UAS-LacZ^{RNAi}; mito-QC/+
USP30^{RNAi}	Mef2-GAL4/UAS-USP30^{RNAi}; mito-QC/+
B	
Control	Mef2-GAL4/UAS-LacZ^{RNAi}; mito-QC/+
USP30^{RNAi}	Mef2-GAL4/UAS-USP30^{RNAi}; mito-QC/+
C	
Control	UAS-LacZ^{RNAi}/+; da-GAL4/+
USP30^{RNAi}	UAS-USP30^{RNAi}/+; da-GAL4/+
Control	UAS-LacZ^{RNAi}/+; nSyb-GAL4/+
USP30^{RNAi}	UAS-USP30^{RNAi}/+; nSyb-GAL4/+
D	
Control	Act-GAL4/UAS-LacZ
USP30 O/E + LacZ	Act-GAL4, UAS-USP30/UAS-LacZ
USP30 O/E + parkin O/E	Act-GAL4, UAS-USP30/UAS-parkin
USP30 O/E + March5 O/E	Act-GAL4, UAS-USP30/+; UAS-March5/+
USP30 O/E + Mul1 O/E	Act-GAL4, UAS-USP30/+; UAS-Mul1/+
E	
Control	mito-QC/UAS-LacZ^{RNAi}; nSyb-GAL4/+
parkin O/E	mito-QC/UAS- parkin$_{C2}$; nSyb-GAL4/+
F	
Control	mito-QC/UAS-LacZ^{RNAi}; nSyb-GAL4/+

parkin O/E	mito-QC/UAS- parkin$_{C2}$; nSyb-GAL4/+
G	
Control	mito-QC/+; nSyb-GAL4/+
Mul1$^{-/-}$	mito-QC/+; nSyb-GAL4, Mul1[A6]/Mul1[A6]
H	
Control	mito-QC/+; nSyb-GAL4/+
Mul1$^{-/-}$	mito-QC/+; nSyb-GAL4, Mul1[A6]/Mul1[A6]
I	
Control	mito-QC/UAS-LacZ^{RNAi}; nSyb-GAL4/+
March5$^{RNAi\ KK}$	mito-QC/UAS-March5$^{RNAi\ KK}$; nSyb-GAL4/+
March5$^{RNAi\ GD}$	mito-QC/UAS-March5$^{RNAi\ GD}$; nSyb-GAL4/+
J	
Control	mito-QC/UAS-LacZ^{RNAi}; nSyb-GAL4/+
March5$^{RNAi\ KK}$	mito-QC/UAS-March5$^{RNAi\ KK}$; nSyb-GAL4/+
March5$^{RNAi\ GD}$	mito-QC/UAS-March5$^{RNAi\ GD}$; nSyb-GAL4/+

Supplementary Figure 4	
Label	**Genotype**
A	
Control	mito-QC/UAS-LacZ^{RNAi}; nSyb-GAL4/+
Atg8a$^{-/-}$, USP30^{RNAi}	Atg8a[KG07569]/Y; mito-QC/UAS-USP30^{RNAi}; nSyb-GAL4/+
Atg8a$^{-/-}$, ntc O/E	Atg8a[KG07569]/Y; mito-QC/UAS-ntc; nSyb-GAL4/+
Atg8a$^{-/-}$, ntc$^{-/-}$	Atg8a[KG07569]/Y; mito-QC/ LacZ^{RNAi}; nSyb-GAL4, ntc^{ms771}/ntc^{ms771}
B	
Control	mito-QC/UAS-LacZ^{RNAi}; nSyb-GAL4/+

Atg8a$^{-/-}$, USP30^{RNAi}	Atg8a[KG07569]/Y; mito-QC/UAS-USP30^{RNAi}; nSyb-GAL4/+
Atg8a$^{-/-}$, ntc O/E	Atg8a[KG07569]/Y; mito-QC/UAS-ntc; nSyb-GAL4/+
Atg8a$^{-/-}$, ntc$^{-/-}$	Atg8a[KG07569]/Y; mito-QC/ LacZ^{RNAi}; nSyb-GAL4, ntc^{ms771}/ntc^{ms771}
C	
Control	mito-QC/UAS-LacZ^{RNAi}; nSyb-GAL4/+
park$^{-/-}$	mito-QC/UAS-LacZ^{RNAi}; nSyb-GAL4, park^{25}/park^{25}
USP30^{RNAi}, park$^{-/-}$	mito-QC/UAS-USP30^{RNAi}; nSyb-GAL4, park^{25}/park^{25}
Atg8a$^{-/-}$, USP30^{RNAi}, park$^{-/-}$	Atg8a[KG07569]/Y; mito-QC/UAS-USP30^{RNAi}; nSyb-GAL4, park^{25}/park^{25}
D	
Control	mito-QC/UAS-LacZ^{RNAi}; nSyb-GAL4/+
park$^{-/-}$	mito-QC/UAS-LacZ^{RNAi}; nSyb-GAL4, park^{25}/park^{25}
USP30^{RNAi}, park$^{-/-}$	mito-QC/UAS-USP30^{RNAi}; nSyb-GAL4, park^{25}/park^{25}
Atg8a$^{-/-}$, USP30^{RNAi}, park$^{-/-}$	Atg8a[KG07569]/Y; mito-QC/UAS-USP30^{RNAi}; nSyb-GAL4, park^{25}/park^{25}

Supplementary Figure 5	
Label	**Genotype**
A	
Control	UAS-LacZ/+; da-GAL4/+
ntc O/E	UAS-ntc/+; da-GAL4/+
USP30^{RNAi}	UAS-USP30^{RNAi}/+; da-GAL4/+
B	
Control	UAS-LacZ/+; da-GAL4/+
ntc O/E	UAS-ntc/+; da-GAL4/+
USP30^{RNAi}	UAS-USP30^{RNAi}/+; da-GAL4/+

C	
Control	w^{1118}
$ntc^{-/-}$	ntc^{ms771}/ntc^{ms771}